Channel Map-Based Angle Domain Multiple Access for Cell-Free Massive MIMO Communications

Shuaifei Chen, *Member, IEEE*, Cheng-Xiang Wang, *Fellow, IEEE*, Junling Li, *Member, IEEE*, Chen Huang, *Member, IEEE*, Hengtai Chang, *Member, IEEE*, Yusong Huang, Jie Huang, *Member, IEEE*, and Yunfei Chen, *Senior Member, IEEE*

***Abstract*—Being aware of the channel and its properties is critical for coherent transmission in massive multiple-input multiple-output (M-MIMO) systems due to the large channel dimension in the space domain. In cell-free (CF) systems, the channel dimension increases further as each user is served by multiple access points, with a significant burden on signal processing. Angle domain transmission and channel maps promise to alleviate this burden by reducing channel dimensions in the angle domain and providing a priori channel information through channel measurements and modeling, respectively. In this paper, we propose a channel map-based angle domain multiple access scheme for the uplink CF M-MIMO communications. First, we propose an angle domain data reception scheme constituting receive combining and large-scale fading decoding to maximize spectral efficiency. Then, we derive an initial access criterion utilizing the angle domain channel similarity between users, based on which we propose pilot assignment and access point selection schemes for better trade-offs between spectral and energy efficiency. Finally, we construct two channel map-based transmission mechanisms by wielding different levels of channel information, where a tailored data reception scheme with a newly derived spectral efficiency upper bound is also proposed for quantitative evaluation. Simulation results show that the proposed channel map-based angle domain schemes outperform their space domain alternatives and the schemes without using channel maps regarding spectral and energy efficiency.**

***Index Terms*—Cell-free massive MIMO, angle domain, multiple access, channel map, distributed processing.**

Received 22 August 2024; revised 5 December 2024; accepted 16 January 2025. Date of publication 13 February 2025; date of current version 5 May 2025. This work was supported in part by the National Natural Science Foundation of China (NSFC) under Grant 62394290 Grant 62394291, and Grant 62401643, in part by the Fundamental Research Funds for the Central Universities under Grant 2242022k60006, in part by the Young Elite Scientists Sponsorship Program by China Association for Science and Technology (CAST) under Grant 2022QNRC001, and in part by the Research Fund of National Mobile Communications Research Laboratory, Southeast University, under Grant 2024A05. The guest editor coordinating the review of this article and approving it for publication was Dr. Tsung-Hui Chang. Part of this paper was accepted to be presented at the IEEE International Conference on Communications 2025 (ICC 2025). *(Corresponding authors: Cheng-Xiang Wang; Chen Huang.)*

Shuaifei Chen and Chen Huang are with the Purple Mountain Laboratories, Nanjing 211111, China, and also with the National Mobile Communications Research Laboratory, School of Information Science and Engineering, Southeast University, Nanjing 211189, China (e-mail: shuaifeichen@seu.edu.cn; huangchen@pmlabs.com.cn).

Cheng-Xiang Wang, Junling Li, and Jie Huang are with the National Mobile Communications Research Laboratory, School of Information Science and Engineering, Southeast University, Nanjing 211189, China, and also with the Pervasive Communication Research Center, Purple Mountain Laboratories, Nanjing 211111, China (e-mail: chxwang@seu.edu.cn; junlingli@seu.edu.cn; j_huang@seu.edu.cn).

Hengtai Chang is with the School of Information Science and Engineering, Shandong University, Qingdao 266237, China (e-mail: changht@sdu.edu.cn).

Yusong Huang is with the National Mobile Communications Research Laboratory, School of Information Science and Engineering, Southeast University, Nanjing 211189, China (e-mail: huang_ys@seu.edu.cn).

Yunfei Chen is with the Department of Engineering, University of Durham, DH1 3LE Durham, U.K. (e-mail: yunfei.chen@durham.ac.uk).

Digital Object Identifier 10.1109/JSTSP.2025.3536289

I. Introduction

LOOKING towards 2030 and beyond, sixth-generation (6G) mobile communication systems are envisioned to initialize a "global coverage, all spectra, full applications, all senses, all digital, and strong security" communication era [2]. Compared to fifth-generation (5G) systems, 6G systems are expected to have a much denser and more flexible network infrastructure with a dramatically increased number of access points (APs) and user equipment (UE). Each node might be equipped with a large antenna array to perform diverse and delicate signal processing tasks, resulting in a tenfold and even hundredfold system transmission performance improvement indicated by spectral efficiency (SE), energy efficiency (EE), connection density, latency, etc [3]. This improvement could be achieved by employing and integrating new enabling technologies, such as cell-free (CF) massive multiple-input multiple-output (M-MIMO) [4], ultra-M-MIMO [5] with electromagnetic information theory [6], integrated sensing and communication, millimeter wave/terahertz transmission, and artificial intelligence-enabled transmission. Among these candidates for 6G, CF M-MIMO has attracted extensive attention from academia and industry in the past few years due to its benefits from both the network and radio access perspectives in multiple access scenarios. Specifically, as illustrated in Fig. 1, CF M-MIMO achieves a user-centric networking, allowing each UE to be served by multiple APs coordinated by a central processing unit (CPU) rather than only one AP as in cellular M-MIMO systems. This eliminates the inevitable inter-cell interference of cellular M-MIMO and provides almost uniform service to all UEs by offering more freedom for cooperative signal processing among APs. From the radio access perspective, CF M-MIMO inherits the proven signal processing techniques from cellular M-MIMO by equipping multiple antennas per AP and enhances the so-called *macro-diversity gain* by shortening average AP-UE distances.

The distributed nature of CF M-MIMO leads to the featured two-stage approach for signal processing [7]. Taking the uplink transmission as an example, the pilot and data signals

from UEs are pre-processed at the local APs in a distributed manner and then gathered at the CPU for final processing by weighted soft combining. The distributed pre-processing at APs can be designed to minimize the local channel estimate and data mean-squared-error (MSE) during channel estimation and data decoding, respectively. Since the weight design at the CPU only exploits the large-scale fading (LSF) coefficients, this distributed approach is known as the LSF decoding (LSFD) in the uplink [8] and the LSF precoding in the downlink [9]. Compared to the centralized approach, where the CPU is responsible for all processing tasks and the APs only play the role of relays, the distributed approach achieves a comparable user experience data rate, i.e., the 95% -likely SE indicating the SE can be achieved by 95% of UEs, but with much lower computational complexity.

Besides, the distributed AP deployment topology brings new opportunities and challenges for the initial access design for CF M-MIMO, comprising pilot assignment and AP selection [10], [11]. More precisely, each UE is assigned a pilot for channel estimation and served by a subset of influential APs with strong channels during data processing instead of all APs. Determining which AP will serve which UE with which pilot is a combinatorial problem, which can be solved by heuristic approaches compromising transmission performance and computational complexity. For the pilot assignment, random assignment and greedy assignment are the most commonly used approaches [7]. The former assigns each UE to a randomly selected pilot, and the latter refines the SE of the weakest UE by iterative pilot updating while the global optimal cannot be guaranteed. Exploiting more elaborate schemes, such as graph theory-based [12] and genetic algorithm-based [13] schemes, can improve the assignment performance, but at the price of high complexity. The AP selection is affected by pilot assignment since an AP serves at most one UE per pilot from causing substantial pilot contamination. Hence, the most intuitive AP selection scheme is that each AP serves τ_{p} UEs with the strongest channels, where τ_{p} is the number of available pilot sequences. This simple greedy approach maximizes the system's utility with the risk that UEs with weak channels might not be served. To achieve a better AP-UE association, the matching theory [14] was used to associate each UE with at least one AP with the maximum association quota τ_{p} for each AP. Although the aforementioned schemes perform well in their respective target scenarios, they operate in the space domain while the practical data streams are propagated as beams in the angle domain. Moreover, these schemes usually ignore the environment-related channel state information (CSI) that can be exploited to assist the transmission. Therefore, the transmission performance still has room for improvement by being aware of the channel and benefiting the properties.

The angle domain channel model [15], also known as the beam domain channel model, has been applied to M-MIMO communications with many successful cases, e.g., multiple access [16], [17], channel estimation [18], [19], [20], beam scheduling [21], unmanned aerial vehicle (UAV) communications [22], [23], etc. The benefits are mainly twofold. On the one hand, projecting the transmission design from the space domain into the angle domain reduces the processing complexity due to the reduced channel dimension [15]. It enjoys the comparable accuracy and pervasiveness of the corresponding space domain channel models, e.g., the conventional correlated Rayleigh and Rician fading channels and the pioneering 6G pervasive channel model (6GPCM) [24], [25]. On the other hand, the natural channel sparsity in the angle domain can be exploited to identify channel differences between different APs and UEs more prominently [21], which improves the interference suppression and resource allocation qualities in large CF M-MIMO systems with complicated communication node associations. In addition to utilizing the angle domain CSI to highlight channel characteristics, the transmission performance can be further improved by exploiting more accurate CSI refined by the practical propagation environment. Channel map is emerging as an attractive concept and tool that describes the propagation environment-related channel characteristics within a specific geographic area [26]. Working as a site-specific database equipped at the APs or base stations, a channel map takes the geographical locations as inputs and outputs the desired CSI, such as channel gains, path losses, and even the complete channel coefficients [27]. Therefore, the channel map can improve transmission quality with reduced processing complexity thanks to its provided a priori environment-related CSI, and thus, enable a channel map-based transmission for beamforming [28], UAV trajectory planning [29], localization [30], etc. However, to the best of the authors' knowledge, channel map-aided angle domain transmission has not been considered in the literature on CF M-MIMO, where the distributed nature and increased channel dimension yield a substantial burden on signal processing and present a considerable potential for enhanced performance.

To this end, in this paper we propose a channel map-based angle domain multiple access scheme for uplink CF M-MIMO systems. Receive combining, LSFD, pilot assignment, and AP selection schemes are proposed based on the angle domain CSI, which can be obtained from the channel maps [31]. Our main contributions are listed as follows:

- We propose a two-stage data reception scheme that exploits angle domain LSF coefficients for uplink CF M-MIMO. The angle domain receive combining vectors and LSFD vectors are derived to minimize the local data MSE at APs in the first stage and maximize the SE per UE at the CPU in the second stage, respectively.
- We derive an initial access criterion that minimizes the channel estimate normalized MSE (NMSE), guided by which we propose a pilot assignment scheme and an AP selection scheme. The former utilizes the angle domain similarity between UEs for overall interference minimization and the latter employs sparse optimization on the angle domain LSFD vectors for EE improvement.
- We construct two channel map-based transmission mechanisms with different levels of CSI, i.e., the large-scale CSI refined by the practical propagation environment and the perfect complete CSI. An upper bound of the SE expression is proposed for quantitative evaluation. The corresponding MSE-minimizing combining and SE-maximizing LSFD vectors are derived as well.

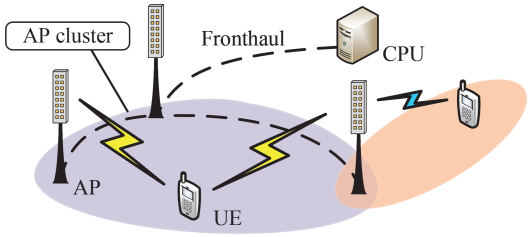

Fig. 1. Considered CF M-MIMO system.

- We compare the proposed angle domain schemes with their space domain alternatives. Simulation results demonstrate that the angle domain schemes improve SE performance and offer a better SE-EE trade-off. Compared to the schemes without using channel maps, the channel map-based schemes further boost transmission performance by exploiting more accurate and additional CSI for transmission scheme design.

The rest of this paper is organized as follows. Section II introduces the considered CF M-MIMO system and channel model. Section III details the angle domain data reception scheme including pilot and date transmission. The angle domain pilot assignment and AP selection are proposed in Section IV. Section V elaborates on the channel map-based transmission mechanisms with a tailored data reception design. Simulation results are provided in Section VI to evaluate the proposed channel map-based angle domain multiple access schemes. Finally, Section VII draws the conclusions.

Notation: The boldface lowercase letters, $\mathbf{x}$, boldface uppercase letters, $\mathbf{X}$, and calligraphic uppercase letters, $\mathcal{A}$, denote the column vectors, matrices, and sets, respectively. The superscripts $(\cdot)^{\mathrm{T}}$, $(\cdot)^{\star}$, $(\cdot)^{\mathrm{H}}$, and $(\cdot)^{\dagger}$, denote the transpose, conjugate, conjugate transpose, and pseudo-inverses, respectively. We denote by $\mathcal{N}_{\mathbb{C}}(\mathbf{0}, \mathbf{R})$ the multi-variate circularly symmetric complex Gaussian distribution with correlation matrix $\mathbf{R}$. We denote by $\mathbf{I}_n$ the $n \times n$ identity matrix and $\|\cdot\|_{\mathrm{F}}$ the Frobenious norm. We use $\mathbb{E}\{\cdot\}$ to compute the expectation values and $\mathsf{Cov}\{\cdot\}$ for the covariance values.

II. System Model

As illustrated in Fig. 1, we consider a CF M-MIMO system with L geographically distributed N-antenna APs and K single-antenna UEs. We assume that each AP is elevated and equipped with a uniform linear array (ULA) with half-wavelength-spaced omnidirectional antennas and each UE is surrounded by dense scatterers.

A. User-Centric CF M-MIMO System

We utilize the two-stage distributed processing approach [7] in a user-centric network, where each UE is served by multiple APs coordinated by a CPU via fronthaul connections for joint signal processing. More precisely, only the final data decoding is handled at the CPU and the other signal processing tasks are performed at the APs. How to determine the association between APs and UEs is discussed in Section IV. For now, we let $\mathcal{D}_l \subset \{1,\ldots,K\}$ denote the set of UEs served by AP l.

We adopt the block fading model with standard time division duplex (TDD) operation, where each time-frequency resource is divided into multiple coherence blocks so that the pilot sequences and payload data can be assumed to transmit in each block with fixed channel coefficients. Each coherence block of τ_{c} channel uses is separated into two segments, where τ_{p} channel uses are dedicated to pilot transmission and channel estimation and the remaining $\tau_{\mathrm{u}} = \tau_{\mathrm{c}} - \tau_{\mathrm{p}}$ channel uses are used for the uplink payload data transmission.

B. Angle Domain Channel Model

We consider the angle domain channel model where the space domain channel transfer function (CTF) between AP l and UE k is denoted by $\mathbf{h}_{kl} \in \mathbb{C}^N$, which can be represented by the corresponding angle domain channel vector $\mathbf{g}_{kl} \in \mathbb{C}^N$ as [22]

$$\mathbf{h}_{kl} = \mathbf{U}\mathbf{g}_{kl} \in \mathbb{C}^N \tag{1}$$

where $\mathbf{U} \in \mathbb{C}^{N\times N}$ is a deterministic matrix of which the columns are the sampled steering vectors of the N angular beams covering the entire angle domain. Recall that the AP antenna arrays are assumed to be half-wavelength-spaced. Then, the sampled steering matrix is expressed as

$$\mathbf{U} = [\mathbf{u}(\omega_1), \ldots, \mathbf{u}(\omega_N)]^{\mathrm{T}} \in \mathbb{C}^{N\times N} \tag{2}$$

where the sampled steering vector is given by [22]

$$\mathbf{u}(\omega_n) = [1, e^{-\jmath\pi\omega_n}, \ldots, e^{-\jmath\pi(N-1)\omega_n}]^{\mathrm{T}} \in \mathbb{C}^N \tag{3}$$

with $\omega_n = \frac{2(n-1)-N}{N}$ being the sampled directional cosines, $n = 1,\ldots,N$. It can be checked that $\mathbf{U}^{\mathrm{H}}\mathbf{U} = N\mathbf{I}_N$.

We consider a narrowband system operating in the angle domain where the received signal at each AP is first transformed to the angle domain and then processed in the digital domain. The angle domain channel vectors are obtained according to (1). According to the multidimensional central limit theorem, the space domain channel $\mathbf{h}_{kl}$ can be drawn from a simplified instance of the 6GPCM [24] as

$$\mathbf{h}_{kl} = \mathbf{h}^{\mathrm{L}}_{kl} e^{\jmath\phi_{kl}} + \mathbf{h}^{\mathrm{N}}_{kl} = \mathbf{U}\mathbf{g}^{\mathrm{L}}_{kl} e^{\jmath\phi_{kl}} + \mathbf{U}\mathbf{g}^{\mathrm{N}}_{kl} \tag{4}$$

when the number of multipath components between AP l and UE k tends to be infinite. The deterministic line-of-sight (LoS) component is denoted by $\mathbf{h}^{\mathrm{L}}_{kl} \in \mathbb{C}^N$ with $\beta^{\mathrm{L}}_{kl} = \frac{1}{N}(\mathbf{h}^{\mathrm{L}}_{kl})^{\mathrm{H}}\mathbf{h}^{\mathrm{L}}_{kl}$ and $\mathbf{g}^{\mathrm{L}}_{kl} \in \mathbb{C}^N$ being its LSF coefficient and angle domain representative, respectively. The phase shift of the LoS component, i.e., $\phi_{kl} \sim \mathcal{U}[-\pi, \pi]$, is uniformly distributed. The stochastic non-LoS (NLoS) components are represented by $\mathbf{h}^{\mathrm{N}}_{kl} \sim \mathcal{N}_{\mathbb{C}}(\mathbf{0}, \mathbf{R}^{\mathrm{N}}_{kl})$ with $\mathbf{R}^{\mathrm{N}}_{kl} = \mathbb{E}\{\mathbf{h}^{\mathrm{N}}_{kl}(\mathbf{h}^{\mathrm{N}}_{kl})^{\mathrm{H}}\} \in \mathbb{C}^{N\times N}$, $\beta^{\mathrm{N}}_{kl} = \frac{1}{N}\mathrm{tr}(\mathbf{R}^{\mathrm{N}}_{kl})$, and $\mathbf{g}^{\mathrm{N}}_{kl} \in \mathbb{C}^N$ being the corresponding covariance matrix, LSF coefficient, and angle domain representative, respectively. Note that the phase shift ϕ_{kl} varies at the same pace as $\mathbf{h}^{\mathrm{L}}_{kl}$ and is assumed to be independent and identically distributed in each coherence block. Accordingly, the covariance matrix of the CTF $\mathbf{h}_{kl}$ is obtained as $\mathbf{R}_{kl} = \mathbb{E}\{\mathbf{h}_{kl}\mathbf{h}^{\mathrm{H}}_{kl}\} = \mathbf{h}^{\mathrm{L}}_{kl}(\mathbf{h}^{\mathrm{L}}_{kl})^{\mathrm{H}} + \mathbf{R}^{\mathrm{N}}_{kl}$ with $\beta_{kl} = \frac{1}{N}\mathrm{tr}(\mathbf{R}_{kl})$ being the corresponding LSF coefficient. Additionally, $\mathbf{\Omega}_{kl} = \mathbb{E}\{\mathbf{g}_{kl}\mathbf{g}^{\mathrm{H}}_{kl}\} = \frac{1}{N^2}\mathbf{U}^{\mathrm{H}}\mathbf{R}_{kl}\mathbf{U} =$

$\mathbf{g}_{kl}^{\mathrm{L}}(\mathbf{g}_{kl}^{\mathrm{L}})^{\mathrm{H}} + \mathbf{\Omega}_{kl}^{\mathrm{N}} \in \mathbb{C}^{N\times N}$ is the covariance matrix of $\mathbf{g}_{kl}$ with $\mathbf{\Omega}_{kl}^{\mathrm{N}} = \mathbb{E}\{\mathbf{g}_{kl}^{\mathrm{N}}(\mathbf{g}_{kl}^{\mathrm{N}})^{\mathrm{H}}\} \in \mathbb{C}^{N\times N}$. The covariance matrices of all UEs $\{\mathbf{R}_{kl} : \forall k\}$ are assumed to be available at AP $l, \forall l$, through channel maps in Section V. This implies that the proposed schemes in this paper are also applicable to ultra-M-MIMO when near-field channel characteristics are represented by the covariance matrices [5].

The LSF coefficient β_{kl} is allocated to the LoS and NLoS components by the location-related Rician K-factor $\kappa_{kl} = p_{kl}^{\mathrm{L}} \cdot 10^{1.3-0.003d_{kl}}$ [32] in linear scale as

$$\beta_{kl}^{\mathrm{L}} = \frac{\kappa_{kl}}{\kappa_{kl}+1}\beta_{kl}, \quad \beta_{kl}^{\mathrm{N}} = \frac{1}{\kappa_{kl}+1}\beta_{kl} \tag{5}$$

where $d_{kl} = \|\mathbf{c}_l^{\mathrm{ap}} - \mathbf{c}_k^{\mathrm{ue}}\|^2 \in \mathbb{R}$ is the distance between AP l and UE k determined by their available three-dimensional (3D) location vectors $\mathbf{c}_l^{\mathrm{ap}} \in \mathbb{R}^3$ and $\mathbf{c}_k^{\mathrm{ue}} \in \mathbb{R}^3$ with $p_{kl}^{\mathrm{L}} \in \{0,1\}$ being the corresponding LoS probability. More precisely, $p_{kl}^{\mathrm{L}} = 1$ indicates the existence of the LoS component and $p_{kl}^{\mathrm{L}} = 0$ when the LoS component does not exist (e.g., blocked by buildings). Therefore, the K-factor κ_{kl} and LoS probability p_{kl}^{L} are strongly related to the location vectors and the practical propagation environment, and further influence the channel $\mathbf{h}_{kl}$. Considering the effects of these environment-related information during the signal processing and initial access will significantly improve the transmission performance quality, thanks to the better match between the designed transmission schemes and the real wireless channels, over which the signal transmissions actually take place. This is elaborated in Section V.

III. Angle Domain Pilot and Data Transmission

In this section, we elaborate the angle domain pilot and data transmission where the angle domain receive combining vectors and LSFD vectors are derived.

A. Channel Estimation via Pilot Transmission

During the uplink pilot phase, each AP locally performs channel estimation based on the received uplink pilots transmitted from the UEs. Each UE is assigned a τ_{p}-length pilot sequence from an orthogonal pilot set with a cardinality of τ_{p}. The pilots must be shared between the UEs since it is likely to have $\tau_{\mathrm{p}} \ll K$ in practical large networks. We denote by ι_k the pilot index assigned to UE k and $\mathcal{S}_{\iota_k}$ the set of UEs sharing pilot ι_k.

When the UEs transmit their pilots, the received pilot signal $\mathbf{y}_{\iota_k l}^{\mathrm{p}} \in \mathbb{C}^N$ at AP l after despreading with pilot ι_k is [33, Section III]

$$\begin{aligned}\mathbf{y}_{\iota_k l}^{\mathrm{p}} &= \sum_{i\in\mathcal{S}_{\iota_k}} \sqrt{\tau_{\mathrm{p}}p_{\mathrm{p}}}\mathbf{h}_{il} + \mathbf{n}_l \\ &= \sqrt{\tau_{\mathrm{p}}p_{\mathrm{p}}}\mathbf{U}\mathbf{g}_{kl} + \sqrt{\tau_{\mathrm{p}}p_{\mathrm{p}}} \sum_{i\in\mathcal{S}_{\iota_k}\setminus\{k\}} \mathbf{U}\mathbf{g}_{il} + \mathbf{n}_l \end{aligned} \tag{6}$$

where p_{p} represents the transmit power for pilots and $\mathbf{n}_l \sim \mathcal{N}_{\mathbb{C}}(\mathbf{0}, \sigma^2\mathbf{I}_N)$ represents the receiver noise with power σ^2.

If the deterministic LoS component $\mathbf{h}_{kl}^{\mathrm{L}}$ is available at AP l while the phase shift ϕ_{kl} is not, the *linear minimum MSE (MMSE)* estimate of $\mathbf{g}_{kl}$ can be derived as [33, Section III]

$$\widehat{\mathbf{g}}_{kl} = \sqrt{\tau_{\mathrm{p}}p_{\mathrm{p}}}\mathbf{\Omega}_{kl}\mathbf{U}^{\mathrm{H}}\mathbf{\Psi}_{\iota_k l}^{-1}\mathbf{y}_{\iota_k l}^{\mathrm{p}} \tag{7}$$

where $\mathbf{\Psi}_{\iota_k l} = \mathbb{E}\{\mathbf{y}_{\iota_k l}^{\mathrm{p}}(\mathbf{y}_{\iota_k l}^{\mathrm{p}})^{\mathrm{H}}\} = \tau_{\mathrm{p}}p_{\mathrm{p}}\sum_{i\in\mathcal{S}_{\iota_k}} \mathbf{U}\mathbf{\Omega}_{il}\mathbf{U}^{\mathrm{H}} + \sigma^2\mathbf{I}_N$ is the correlation matrix of $\mathbf{y}_{\iota_k l}^{\mathrm{p}}$ in (6). Due to the pilot-sharing among the UEs in $\mathcal{S}_{\iota_k}$, $\mathbf{\Psi}_{\iota_k l}$ contains not only the statistical CSI of the desired UE k but also that of the other UEs in $\mathcal{S}_{\iota_k}$, which induces the so-called *pilot contamination* and thus degrades the channel estimation quality. The angle domain channel estimate $\widehat{\mathbf{g}}_{kl}$ and its estimation error $\widetilde{\mathbf{g}}_{kl} = \mathbf{g}_{kl} - \widehat{\mathbf{g}}_{kl}$ are uncorrelated random variables with

$$\mathbb{E}\{\widehat{\mathbf{g}}_{kl}\} = \mathbf{0}, \quad \mathrm{Cov}\{\widehat{\mathbf{g}}_{kl}\} = \mathbf{\Omega}_{kl} - \mathbf{\Xi}_{kl} \tag{8}$$

$$\mathbb{E}\{\widetilde{\mathbf{g}}_{kl}\} = \mathbf{0}, \quad \mathrm{Cov}\{\widetilde{\mathbf{g}}_{kl}\} = \mathbf{\Xi}_{kl} \tag{9}$$

where $\mathbf{\Xi}_{kl} = \mathbf{\Omega}_{kl} - \tau_{\mathrm{p}}p_{\mathrm{p}}\mathbf{\Omega}_{kl}\mathbf{U}^{\mathrm{H}}\mathbf{\Psi}_{\iota_k l}^{-1}\mathbf{U}\mathbf{\Omega}_{kl}$. The linear MMSE estimate of $\mathbf{h}_{kl}$ can be represented as $\widehat{\mathbf{h}}_{kl} = \mathbf{U}\widehat{\mathbf{g}}_{kl}$.

B. Data Transmission With LSFD

We consider the distributed uplink data transmission where the so-called LSFD strategy is employed. Each AP locally performs an arbitrary receive combining scheme to compute local data estimates. Then, these estimates are gathered and combined at the CPU for final decoding by performing LSFD. More precisely, AP l physically receives the data signals from all UEs, which is given by

$$\mathbf{y}_l^{\mathrm{ul}} = \sum_{i=1}^{K} \mathbf{h}_{il}s_i + \mathbf{n}_l \tag{10}$$

where $s_i \in \mathbb{C}$ represents the signal transmitted by UE i with transmit power $p_i = \mathbb{E}\{|s_i|^2\}$ and $\mathbf{n}_l \sim \mathcal{N}_{\mathbb{C}}(\mathbf{0}, \sigma^2\mathbf{I}_M)$ represents the independent additive receiver noise. According to the fractional power control policy [7], [8], the transmit powers $\{p_k, \forall k\}$ can be obtained as

$$p_k = p_{\max}\frac{\min_{i\in\{1,\ldots,K\}}\sqrt{\sum_{l=1}^{L}\mathrm{tr}(\mathbf{D}_{il})\beta_{il}}}{\sqrt{\sum_{l=1}^{L}\mathrm{tr}(\mathbf{D}_{kl})\beta_{kl}}} \tag{11}$$

where $p_{\max}$ is the maximal transmit power of a UE and matrix

$$\mathbf{D}_{kl} = \begin{cases}\mathbf{I}_N, & \text{if } k \in \mathcal{D}_l \\ \mathbf{0}_N, & \text{otherwise}\end{cases} \tag{12}$$

indicates if UE k is served by AP l or not.

AP l first transforms the received signal into the angle domain as $\frac{1}{N}\mathbf{U}^{\mathrm{H}}\mathbf{y}_l^{\mathrm{ul}}$ and then selects the local angle domain combining vector $\mathbf{D}_{kl}\mathbf{v}_{kl} \in \mathbb{C}^N$ for UE k to compute the local estimate of s_k as

$$\widehat{s}_{kl} = \frac{1}{N}\mathbf{v}_{kl}^{\mathrm{H}}\mathbf{D}_{kl}\mathbf{U}^{\mathrm{H}}\mathbf{y}_l^{\mathrm{ul}}. \tag{13}$$

In analogy with the *local MMSE (L-MMSE)* combining scheme [7], we propose an angle domain L-MMSE combining scheme that provides the best local data estimate $\widehat{s}_{kl}$ with minimal conditional MSE $\mathbb{E}\{|s_k - \widehat{s}_{kl}|^2|\{\widehat{\mathbf{g}}_{il} : \forall i\}\}$, which is given in the following lemma.

Lemma 1: At AP l, the local conditional data MSE for UE k is minimized by the angle domain L-MMSE combining vector

$$\mathbf{v}_{kl}^{\mathrm{l-mmse}} = p_k \left(\sum_{i=1}^{K} p_i \left(\widehat{\mathbf{g}}_{il} \widehat{\mathbf{g}}_{il}^{\mathrm{H}} + \boldsymbol{\Xi}_{il} \right) + \frac{\sigma^2}{N} \mathbf{I}_N \right)^{-1} \mathbf{D}_{kl} \widehat{\mathbf{g}}_{kl}. \tag{14}$$

Proof: This can be proved by computing the conditional expectation and letting $\partial \mathbb{E}\{|s_k - \widehat{s}_{kl}|^2 | \{\widehat{\mathbf{g}}_{il} : \forall i\}\} / \partial \mathbf{v}_{kl} = 0$. ■

The computational complexity of the angle domain L-MMSE combining scheme grows with the UE number K, which leads to an unacceptable computational burden. Inspired by the *local partial MMSE (LP-MMSE)* combining scheme [10], we propose the angle domain LP-MMSE combining scheme as

$$\mathbf{v}_{kl}^{\mathrm{lp-mmse}} = p_k \left(\sum_{i \in \mathcal{D}_l} p_i \left(\widehat{\mathbf{g}}_{il} \widehat{\mathbf{g}}_{il}^{\mathrm{H}} + \boldsymbol{\Xi}_{il} \right) + \frac{\sigma^2}{N} \mathbf{I}_n \right)^{-1} \mathbf{D}_{kl} \widehat{\mathbf{g}}_{kl} \tag{15}$$

in which AP l only exploits the channel estimates and statistics of its serving UEs in $\mathcal{D}_l$ for interference suppression. Since the UEs in $\mathcal{D}_l$ generate the most dominated interference to AP l during the data detection, the angle domain LP-MMSE combining scheme will achieve almost the same interference suppression capability as the optimal angle domain L-MMSE combining scheme in (14) but with limited and much lower computational complexity. Apart from the aforementioned MMSE-type combining schemes, the maximum ratio combining scheme with $\mathbf{v}_{kl}^{\mathrm{mr}} = \mathbf{D}_{kl} \widehat{\mathbf{g}}_{kl}$ can be alternatively used.

Next, the CPU performs the final decoding of s_k by linearly combining the local soft estimates forwarded by the APs. We denote by $\mathbf{b}_{ki} = [\mathbf{v}_{k1}^{\mathrm{H}} \mathbf{D}_{k1} \mathbf{g}_{i1}, \ldots, \mathbf{v}_{kL}^{\mathrm{H}} \mathbf{D}_{kL} \mathbf{g}_{iL}]^{\mathrm{T}} \in \mathbb{C}^L$ the angle domain receive-combined channels from UE i when receiving signals from UE k, and $\mathbf{a}_k = [a_{k1}, \ldots, a_{kL}]^{\mathrm{T}} \in \mathbb{C}^L$ the LSFD weight vector of UE k, where $a_{kl} \in \mathbb{C}$ is the weight corresponding to $\widehat{s}_{kl}$. Then, we can obtain the final estimate of s_k as

$$\widehat{s}_k = \sum_{l=1}^{L} a_{kl}^{\star} \widehat{s}_{kl} = \underbrace{\mathbf{a}_k^{\mathrm{H}} \mathbb{E}\{\mathbf{b}_{kk}\} s_k}_{\text{Desired signal}} + \underbrace{(\mathbf{a}_k^{\mathrm{H}} \mathbf{b}_{kk} - \mathbf{a}_k^{\mathrm{H}} \mathbb{E}\{\mathbf{b}_{kk}\}) s_k + \sum_{i=1, i \neq k}^{K} \mathbf{a}_k^{\mathrm{H}} \mathbf{b}_{ki} s_i}_{\text{Interference}} + \underbrace{n_k'}_{\text{Noise}} \tag{16}$$

where $n_k' = \frac{1}{N} \sum_{l=1}^{L} a_{kl}^{\star} \mathbf{v}_{kl}^{\mathrm{H}} \mathbf{D}_{kl} \mathbf{U}^{\mathrm{H}} \mathbf{n}_l$ is the resulting noise. The LSFD vectors $\{\mathbf{a}_k : \forall k\}$ are selected as a deterministic function of the channel statistics at the CPU where the average effective uplink channel $\mathbb{E}\{\mathbf{a}_k^{\mathrm{H}} \mathbf{b}_{kk}\} = \mathbf{a}_k^{\mathrm{H}} \mathbb{E}\{\mathbf{b}_{kk}\}$ is deterministic and non-zero if the aforementioned combiners are selected and employed.

C. Spectral and Energy Efficiency

Based on (16) and by treating interference as noise, the achievable uplink SE can be quantified by using the *hardening bound* [33, Thm. 4.4] as

$$\mathsf{SE}_k^{\mathrm{ul}} = \frac{\tau_{\mathrm{u}}}{\tau_{\mathrm{c}}} \log_2 \left(1 + \mathsf{SINR}_k^{\mathrm{ul}} \right) \quad \text{bit/s/Hz} \tag{17}$$

where

$$\mathsf{SINR}_k^{\mathrm{ul}} = \frac{p_k |\mathbf{a}_k^{\mathrm{H}} \mathbb{E}\{\mathbf{b}_{kk}\}|^2}{\mathbf{a}_k^{\mathrm{H}} \left(\sum_{i=1}^{K} p_i \mathbb{E}\{\mathbf{b}_{ki} \mathbf{b}_{ki}^{\mathrm{H}}\} - p_k \mathbb{E}\{\mathbf{b}_{kk}\} \mathbb{E}\{\mathbf{b}_{kk}^{\mathrm{H}}\} + \mathbf{F}_k \right) \mathbf{a}_k} \tag{18}$$

is the effective uplink signal-to-interference-plus-noise ratio (SINR) [7, Thm. 5.4] in angle domain with

$$\mathbf{F}_k = \frac{\sigma^2}{N} \mathrm{diag}(\mathbb{E}\{\|\mathbf{D}_{k1} \mathbf{v}_{k1}\|^2\}, \ldots, \mathbb{E}\{\|\mathbf{D}_{kL} \mathbf{v}_{kL}\|^2\}). \tag{19}$$

With the fact that the effective uplink SINR in (18) is a generalized Rayleigh quotient of $\mathbf{a}_k$, the optimal LSFD weight vector that maximizes the effective uplink SINR is given by

$$\mathbf{a}_k^{\mathrm{opt}} = p_k \left(\sum_{i=1}^{K} p_i \mathbb{E}\{\mathbf{b}_{ki} \mathbf{b}_{ki}^{\mathrm{H}}\} + \mathbf{F}_k \right)^{\dagger} \mathbb{E}\{\mathbf{b}_{kk}\} \tag{20}$$

with the help of [33, Lem. B.10] and [33, Lem. B.4]. The resulting maximum SINR value is $\mathsf{SINR}_k^{\mathrm{ul}} = p_k \mathbb{E}\{\mathbf{b}_{kk}^{\mathrm{H}}\} (\sum_{i=1}^{K} p_i \mathbb{E}\{\mathbf{b}_{ki} \mathbf{b}_{ki}^{\mathrm{H}}\} - p_k \mathbb{E}\{\mathbf{b}_{kk}\} \mathbb{E}\{\mathbf{b}_{kk}^{\mathrm{H}}\} + \mathbf{F}_k)^{\dagger} \mathbb{E}\{\mathbf{b}_{kk}\}$. It can be checked that the computational complexity of the optimal LSFD is not scalable with respect to the number of UEs K. Inspired by the *partial LSFD* vector [7], [8], we propose the angle domain partial LSFD vector to approximate the optimal LSFD vector $\mathbf{a}_k^{\mathrm{opt}}$ with scalable computational complexity as

$$\mathbf{a}_k^{\mathrm{par}} = p_k \left(\sum_{i \in \mathcal{P}_k} p_i \mathbb{E}\{\mathbf{b}_{ki} \mathbf{b}_{ki}^{\mathrm{H}}\} + \mathbf{F}_k \right)^{\dagger} \mathbb{E}\{\mathbf{b}_{kk}\} \tag{21}$$

where set $\mathcal{P}_k$ includes the UEs having at least one common serving AP with UE k.

In addition to SE, which indicates the achievable data rates, EE is another essential performance metric considering energy consumption, which is defined as [9], [33]

$$\mathsf{EE} = \frac{B \cdot \sum_{k=1}^{K} \mathsf{SE}_k^{\mathrm{ul}}}{P_{\mathrm{tot}}} \quad \text{bit/Joule} \tag{22}$$

where B represents the system bandwidth and the total power consumption P_{tot} consists of the power consumed at the UEs $\{P_k^{\mathrm{ue}} : \forall k\}$, the active APs $\{P_l^{\mathrm{ap}} : \forall l\}$, fronthaul connections $\{P_l^{\mathrm{fh}} : \forall l\}$, and the CPU P_{cpu} [9]

$$P_{\mathrm{tot}} = \sum_{k=1}^{K} P_k^{\mathrm{ue}} + \sum_{l=1}^{L} P_l^{\mathrm{ap}} + \sum_{l=1}^{L} P_l^{\mathrm{fh}} + P_{\mathrm{cpu}}. \tag{23}$$

The total power consumption is affected by the AP-UE serving relationship. Detailed definitions of each term in (23) can be found in [9] and omitted due to limited space.

IV. Angle Domain Pilot Assignment and AP Selection

In this section, we propose an angle domain initial access strategy considering pilot assignment and AP selection, which are tightly coupled since an AP can only reasonably serve at most one UE per pilot to prevent the weaker pilot-sharing UEs from strong interference. A pilot assignment scheme assigns each UE

with one pilot sequence aiming to mitigate pilot contamination caused by pilot-sharing and thus improve the channel estimation quality and the resulting SE. An AP selection scheme selects at least one serving AP for each UE aiming to refine the multi-AP collaborative signal processing and avoid the unnecessary power consumptions.

A. Access Criterion With Minimized NMSE

Before we delve into the angle domain pilot assignment and AP selection design, we first derive an initial access criterion with the goal of minimizing the NMSE of the channel estimates (abbreviated as NMSE). More precisely, in the considered user-centric CF system, the collective channel $\mathbf{h}_k = [\mathbf{h}_{k1}^{\mathrm{T}}, \ldots, \mathbf{h}_{kL}^{\mathrm{T}}]^{\mathrm{T}} \in \mathbb{C}^{LN}$ of UE k is first locally estimated by its serving APs and then delivered to the CPU, in which its estimate is formed as

$$\mathbf{D}_k \widehat{\mathbf{h}}_k = [(\mathbf{D}_{k1}\widehat{\mathbf{h}}_{k1})^{\mathrm{T}}, \ldots, (\mathbf{D}_{kL}\widehat{\mathbf{h}}_{kL})^{\mathrm{T}}]^{\mathrm{T}}, \ \forall k \tag{24}$$

with $\mathbf{D}_k = \mathrm{diag}(\mathbf{D}_{k1}, \ldots, \mathbf{D}_{kL}) \in \mathbb{C}^{LN \times LN}$ and $\widehat{\mathbf{h}}_k = [\widehat{\mathbf{h}}_{k1}^{\mathrm{T}}, \ldots, \widehat{\mathbf{h}}_{kL}^{\mathrm{T}}]^{\mathrm{T}} \in \mathbb{C}^{LN}$. Then, the NMSE of the collective channel estimate $\mathbf{D}_k\widehat{\mathbf{h}}_k$ is given by

$$\begin{aligned} \mathsf{NMSE}_k &= \frac{\mathbb{E}\{\|\mathbf{D}_k\mathbf{h}_k - \mathbf{D}_k\widehat{\mathbf{h}}_k\|^2\}}{\mathbb{E}\{\|\mathbf{D}_k\mathbf{h}_k\|^2\}} \\ &= 1 - \frac{\tau_{\mathrm{p}} p_{\mathrm{p}} \sum_{l=1}^{L} \mathrm{tr}(\mathbf{D}_{kl}\mathbf{\Omega}_{kl}\mathbf{U}^{\mathrm{H}}\mathbf{\Psi}_{\iota_k l}^{-1}\mathbf{U}\mathbf{\Omega}_{kl})}{\sum_{l=1}^{L}\mathrm{tr}(\mathbf{D}_{kl}\mathbf{\Omega}_{kl})}. \end{aligned} \tag{25}$$

Recall that the pilot contamination is induced by the statistical CSI of the undesired UEs contained in $\mathbf{\Psi}_{\iota_k l}$. Inspired by this, a lower bound of the NMSE in (25) of UE k can be obtained if NMSE_k is only related to its own statistical CSI, which is elaborated in the following lemma.

Lemma 2: Considering a CF M-MIMO system over the angle domain channels, the NMSE in (25) is lower bounded as

$$\begin{aligned} \mathsf{NMSE}_k &\geq \underline{\mathsf{NMSE}}_k \\ &= 1 - \frac{\tau_{\mathrm{p}} p_{\mathrm{p}} \sum_{l=1}^{L} \mathrm{tr}(\mathbf{D}_{kl}\mathbf{\Omega}_{kl}\mathbf{U}^{\mathrm{H}}\widetilde{\mathbf{\Psi}}_{\iota_k l}^{-1}\mathbf{U}\mathbf{\Omega}_{kl})}{\sum_{l=1}^{L}\mathrm{tr}(\mathbf{D}_{kl}\mathbf{\Omega}_{kl})} \end{aligned} \tag{26}$$

where $\widetilde{\mathbf{\Psi}}_{\iota_k l} = \tau_{\mathrm{p}} p_{\mathrm{p}} \mathbf{U}\mathbf{\Omega}_{kl}\mathbf{U}^{\mathrm{H}} + \sigma^2\mathbf{I}_N$. For any l and $i \neq k$, the equality in (26) occurs when one of the following conditions is satisfied

1) $\mathbf{D}_{kl}\mathbf{\Omega}_{kl}\mathbf{\Omega}_{il} = \mathbf{0}$,
2) $\mathbf{D}_{kl}\mathbf{\Omega}_{kl}\mathbf{\Omega}_{il} \neq \mathbf{0}$, $\iota_k \neq \iota_i$.

Proof: The details are relegated to Appendix A. ■

Note that $\mathbf{D}_{kl}\mathbf{\Omega}_{kl}\mathbf{\Omega}_{il} = \mathbf{0}$ occurs when the angle domain channels $\mathbf{g}_{kl}$ and $\mathbf{g}_{il}$ are *non-overlapping* and/or UE k and UE i are not served by AP l simultaneously. Therefore, Lemma 2 implies that for UE k, AP l, and another UE i, $\forall i \neq k$, NMSE_k is approaching $\underline{\mathsf{NMSE}}_k$ if AP l: 1) can directly separate UE k with the other UEs when $\mathbf{\Omega}_{kl}\mathbf{\Omega}_{il} = \mathbf{0}$; 2) or serves UE k and the other UEs with different pilots such the UEs can separated during the despreading when $\mathbf{\Omega}_{kl}\mathbf{\Omega}_{il} \neq \mathbf{0}$; 3) or does not serve UE k and the other UEs at the same time, which is dedicated to CF systems. To characterize the degree of overlap between the UEs in the angle domain when each UE is served by multiple APs, a metric referred to as *similarity* is defined as

$$\rho_{ki} = \frac{\sum_{l=1}^{L}\mathrm{tr}(\mathbf{D}_{kl}\mathbf{\Omega}_{kl}\mathbf{D}_{il}\mathbf{\Omega}_{il})}{\sqrt{\sum_{l=1}^{L}\|\mathbf{D}_{kl}\mathbf{\Omega}_{kl}\|_{\mathrm{F}}^2}\sqrt{\sum_{l=1}^{L}\|\mathbf{D}_{il}\mathbf{\Omega}_{il}\|_{\mathrm{F}}^2}}, \ \forall k, i. \tag{27}$$

Therefore, a criterion for the AP selection and pilot assignment design in the angle domain can be obtained as follows:

- For the considered CF M-MIMO system, given each UE is served by at least one AP, the angle domain similarity of the pilot-sharing UEs should be as low as possible.

B. Similarity-Based Pilot Assignment

Based on the angle domain similarities defined in (27), we formulate the pilot assignment as a max-K cut problem,

$$\mathsf{P}_1: \ \max_{\{\mathcal{S}_\iota : \iota = 1, \ldots, \tau_{\mathrm{p}}\}} \sum_{1 \leq \iota < \iota' \leq \tau_{\mathrm{p}}} \sum_{i \in \mathcal{S}_\iota, j \in \mathcal{S}_{\iota'}} \rho_{ij}. \tag{28}$$

where the overall inter-set angle domain similarities $\sum_{1\leq\iota<\iota'\leq\tau_{\mathrm{p}}}\sum_{i\in\mathcal{S}_\iota, j\in\mathcal{S}_{\iota'}}\rho_{ki}$ is maximized by properly allocating the UEs into τ_{p} sets, i.e., $\mathcal{S}_1, \ldots, \mathcal{S}_{\tau_{\mathrm{p}}}$. In other words, solving P_1 minimizes the overall intra-set angle domain similarities, i.e., the overall angle domain similarities of the pilot-sharing UEs in the system, since we assign the UEs in the same set with the same pilot. This implies that the overall pilot contamination is minimized as well.

Since P_1 is a combinatorial problem, the complexity of evaluating all $(\tau_{\mathrm{p}})^K$ possible assignments grows exponentially with the number of UEs K, which is infeasible in practical large networks. Therefore, we employ a suboptimal heuristic algorithm [34], which provides an approximate solution as the brute-force approach but in polynomial time. The algorithm proceeds as follows.

1) The first τ_{p} UEs are assigned to τ_{p} mutually orthogonal pilots with $|\mathcal{S}_\iota| = 1$, $\forall \iota$.
2) An arbitrary remaining UE k computes $\rho_k^\iota = \sum_{i\in\mathcal{S}_\iota\cup\{k\}}\rho_{ki}$, $\iota = 1, \ldots, \tau_{\mathrm{p}}$ according to (27). Since the AP selection is not performed yet, we replace $\mathbf{D}_{kl}$ in (27) by

$$\widetilde{\mathbf{D}}_{kl} = \begin{cases} \mathbf{I}_N, & \text{if } k \in \widetilde{\mathcal{D}}_l \\ \mathbf{0}_N, & \text{otherwise} \end{cases} \tag{29}$$

where set $\widetilde{\mathcal{D}}_l$ includes τ_{p} UEs with the largest values of LSF coefficients to AP l.
3) Assign UE k to pilot

$$\iota' = \arg\min_\iota \rho_k^\iota \tag{30}$$

and update $\mathcal{S}_{\iota'} \leftarrow \mathcal{S}_{\iota'} \cup \{k\}$.
4) Repeat steps 2) and 3) until all UEs have been assigned to a pilot.

C. Sparsity-Induced AP Selection

Recall that the optimal angle domain LSFD vector $\mathbf{a}_k^{\mathrm{opt}}$ in (20) is not energy-efficient by letting all AP serve all UEs and the partial angle domain LSFD vector $\mathbf{a}_k^{\mathrm{par}}$ in (21) is suboptimal

without taking the AP selection as a part of the LSFD design. By noticing that $\mathbf{a}_k^{\text{opt}}$ is typically "sparse" with a small number of large elements and many small elements due to the natural path loss differences between distributed located APs and UEs, we formulate the AP selection as a Lasso problem [35]

$$\mathsf{P}_2: \quad \min_{\mathbf{a}_k \in \mathbb{C}^L} \mathsf{MSE}_k + \lambda \|\mathbf{a}_k\|_1, \ k = 1, \ldots, K \tag{31}$$

and the AP selection indication matrix $\mathbf{D}_{kl}$ is obtained according to optimized LSFD vector $\mathbf{a}_k$ as $\mathbf{D}_{kl} = \mathbf{I}_N$ if $a_{kl} \geq 0$ and $\mathbf{D}_{kl} = \mathbf{0}$ otherwise. The first term in (31)

$$\begin{aligned}\mathsf{MSE}_k &= \mathbb{E}\{|s_k - \widehat{s}_k|^2 | \{\widehat{\mathbf{g}}_{il} : \forall i\}\} \\ &= \mathbf{a}_k^{\mathrm{H}} \left(\sum_{i=1}^{K} p_i \mathbb{E}\{\mathbf{b}_{ki} \mathbf{b}_{ki}^{\mathrm{H}}\} + \mathbf{F}_k \right) \mathbf{a}_k - 2 p_k \Re(\mathbf{a}_k^{\mathrm{H}} \mathbb{E}\{\mathbf{b}_{kk}\}) + p_k\end{aligned} \tag{32}$$

represents the MSE cost regarding to the data estimate $\widehat{s}_k$, where the L-MMSE combining vectors $\{\mathbf{v}_{kl}^{\text{l-mmse}} : \forall l\}$ in (14) are used in $\mathbf{b}_{ki}$. The second term in (31) is a ℓ_1-norm penalty, which induces sparsity on $\mathbf{a}_k$ by enforcing a number of elements of $\mathbf{a}_k$ to 0 depending on a tunable regularization parameter $\lambda \geq 0$. A lager value of λ implies more sparsity, and thus reduces the average number of serving UEs per AP from an AP selection perspective. It can be checked that the SINR-maximizing LSFD vector $\mathbf{a}_k^{\text{opt}}$ also minimizes MSE_k. Therefore, solving P_2 maximizes the SE performance by designing the proper LSFD vector $\mathbf{a}_k$ with a certain degree of sparsity induced by the ℓ_1-norm penalty. Since the unnecessary serving relationships are removed with an appropriate λ, the total power consumption is reduced and thus a higher EE can be achieved given the SE loss is marginal.

With the fact that both the MSE cost MSE_k and the ℓ_1-norm penalty $\|\mathbf{a}_k\|_1$ are convex functions with respect to $\mathbf{a}_k$, the well-used optimization tool CVX [36] can be employed to solve P_2. Alternatively, the proximal methods [35] are also applicable for solving P_2 efficiently due to the non-smoothness of $\|\mathbf{a}_k\|_1$.

V. Channel Map-Based Multiple Access Transmission

The capability of distinguishing between UEs that likely cause severe interference is improved by projecting the channels from the space domain into the angle domain due to the natural channel sparsity in the angle domain. System performances like SE and EE are thus enhanced thanks to the reformative angle domain signal processing and initial access schemes, verifying the positive effects obtained by exploiting the appropriate acquired CSI for coherent transmission in the considered CF M-MIMO system. Bearing this in mind, the transmission performance can be further boosted by improving the CSI acquisition quality. This can be achieved by considering the practical propagation environment, which is generally ignored in conventional channel estimation schemes.

Recall that a channel map serves as a site-specific database that maps the geographical locations to the desired CSI, e.g., LoS probability, Rician K-factor, channel gains, etc. Using channel model $\mathbf{h}_{kl} = \mathbf{h}_{kl}^{\mathrm{L}} e^{\jmath \phi_{kl}} + \mathbf{h}_{kl}^{\mathrm{N}}$ in (4), in this section, we propose two channel map-based transmission mechanisms aided by different levels of CSI, namely partial channel map (PCM) and full channel map (FCM), respectively. The former outputs the large-scale CSI of $\mathbf{h}_{kl}$ including $\mathbf{h}_{kl}^{\mathrm{L}}$ and $\mathbf{R}_{kl}^{\mathrm{N}}$, by providing an accurate LoS probability based on the location vectors with practical building layouts. The latter is the ultimate form of channel maps where the complete channel coefficients in $\mathbf{h}_{kl}$ are available by further providing the small-scale CSI $\mathbf{h}_{kl}^{\mathrm{N}}$ and $e^{\jmath \phi_{kl}}$ on the basis of the PCM. Note that FCM serves as the performance upper bound of the channel map-based transmissions since accurate phase shifts $\{e^{\jmath \phi_{kl}} : \forall k, l\}$ are only ideal in practice. The procedure of channel map-based multiple access transmission is demonstrated in Fig. 2, where the complete channel vectors $\{\mathbf{h}_{kl}\}$ or $\{\mathbf{g}_{kl}\}$ are regarded as the "ground-truth" CSI when computing the SE and the acquired CSI obtained with or without channel maps are used to design the transmission schemes including receive combining, LSFD, pilot assignment, and AP selection. The details are elaborated as follows.

A. Large-Scale CSI-Aware Transmission via PCM

The considered PCM $\mathcal{M}_{\text{PCM}}$ can be expressed as a mapping from the current 3D location vectors $(\mathbf{c}_l^{\text{ap}}, \mathbf{c}_k^{\text{ue}})$ of the desired AP-UE pair (l, k) to the corresponding large-scale CSI $\mathbf{h}_{kl}^{\mathrm{L}}$ and $\mathbf{R}_{kl}^{\mathrm{N}}$ by the conditional function $f_{\text{PCM}}(\cdot|\mathcal{E})$, i.e.,

$$\mathcal{M}_{\text{PCM}}: \quad \{\mathbf{h}_{kl}^{\mathrm{L}}, \mathbf{R}_{kl}^{\mathrm{N}}\} = f_{\text{PCM}}((\mathbf{c}_l^{\text{ap}}, \mathbf{c}_k^{\text{ue}})|\mathcal{E}) \tag{33}$$

where $\mathcal{E}$ represents the *environment* database, which can be constructed by approaches like channel measurements and ray-tracing simulations. More precisely, with the half-wavelength-spaced ULA assumption at each AP, the deterministic LoS component $\mathbf{h}_{kl}^{\mathrm{L}}$ is represented as

$$\begin{aligned}\mathbf{h}_{kl}^{\mathrm{L}} = \sqrt{\beta_{kl}^{\mathrm{L}}} \Big[1, e^{\jmath \pi \sin(\varphi_{kl}) \cos(\theta_{kl})}, \\ \ldots, e^{\jmath \pi (N-1) \sin(\varphi_{kl}) \cos(\theta_{kl})}\Big]^{\mathrm{T}}\end{aligned} \tag{34}$$

where φ_{kl} and θ_{kl} are the azimuth angle of arrival (AAoA) and elevation angle of arrival (EAoA) to UE k seen from AP l, respectively. For the covariance matrix of the NLoS components $\mathbf{R}_{kl}^{\mathrm{N}}$, we first let $\bar{\varphi}_{kl} = \varphi_{kl} + \delta_\varphi$ denote the AAoA of a multipath component, where $\delta_\varphi \sim \mathcal{N}(0, \sigma_\varphi^2)$ is a random deviation from φ_{kl} with standard deviation σ_φ. Analogically, $\bar{\theta}_{kl} = \theta_{kl} + \delta_\theta$ denotes the EAoA of a multipath component with a random deviation $\delta_\theta \sim \mathcal{N}(0, \sigma_\theta^2)$. Then, $\mathbf{R}_{kl}^{\mathrm{N}}$ can be generated according to the local scattering model, of which the (m, n)-th element is calculated as [7]

$$[\mathbf{R}_{kl}^{\mathrm{N}}]_{mn} = \beta_{kl}^{\mathrm{N}} \iint e^{\jmath \pi (m-n) \sin(\bar{\varphi}_{kl}) \cos(\bar{\theta}_{kl})} f(\delta_\varphi, \delta_\theta) \mathrm{d}\delta_\varphi \mathrm{d}\delta_\theta \tag{35}$$

where $f(\delta_\varphi, \delta_\theta) = \frac{1}{2\pi\sigma_\varphi\sigma_\theta} e^{-\delta_\varphi^2/(2\sigma_\varphi^2)} e^{-\delta_\theta^2/(2\sigma_\theta^2)}$ is the joint PDF of δ_φ and δ_θ.

The LSF coefficients β_{kl}^{L} in (34) and β_{kl}^{N} in (35) are obtained based on β_{kl} according to the K-factor κ_{kl} and LoS probability p_{kl}^{L} in (5), where β_{kl} is calculated in dB as [32, Table 5.1]

$$\beta_{kl} = \begin{cases} -30.18 - 26 \log_{10}\left(\frac{d_{kl}}{1\mathrm{m}}\right) + F_{kl}^{\mathrm{L}}, & \text{if } p_{kl}^{\mathrm{L}} = 1 \\ -34.53 - 38 \log_{10}\left(\frac{d_{kl}}{1\mathrm{m}}\right) + F_{kl}^{\mathrm{L}}, & \text{otherwise} \end{cases} \tag{36}$$

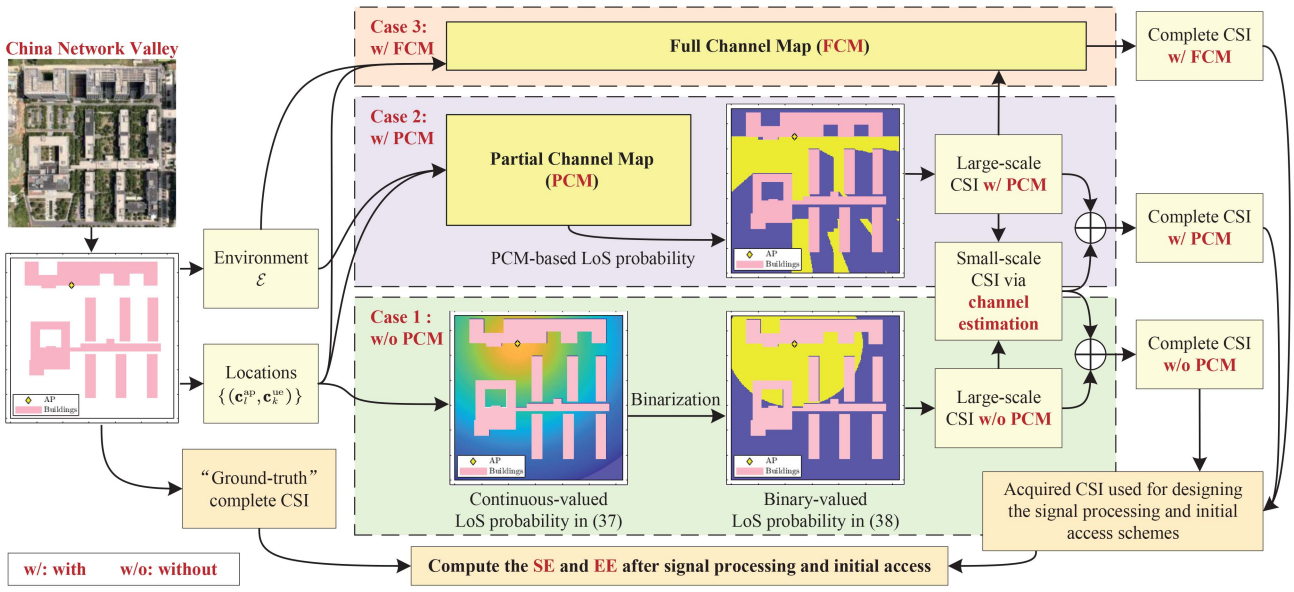

Fig. 2. Procedure of the proposed channel map-based multiple access transmission.

with $F_{kl}^{\rm L} \sim \mathcal{N}(0, 4^2)$ and $F_{kl}^{\rm N} \sim \mathcal{N}(0, 10^2)$ representing the shadow fading in the LoS and NLoS scenarios, respectively. Note that penetration loss is negligible in the studied scenario and so is not considered.

As illustrated in Fig. 2, the LoS probability $p_{kl}^{\rm L}$ can be assumed to be accurately obtained based on the location vectors $(\mathbf{c}_l^{\rm ap}, \mathbf{c}_k^{\rm ue})$ and environment database $\mathcal{E}$ by employing advanced localization methods with powerful data mining capabilities [27]. Alternatively, $p_{kl}^{\rm L}$ can be modelled as a distance-related continuous variable [32]

$$p_{kl}^{\rm L} = \begin{cases} \frac{300 - d_{kl}}{300}, & \text{if } 0 < d_{kl} < 300 \\ 0, & \text{otherwise} \end{cases} \tag{37}$$

with $p_{kl}^{\rm L} \in [0, 1]$, which is irrelevant to the practical propagation environment. To convert the range of $p_{kl}^{\rm L}$ in (37) from [0,1] to $\{0, 1\}$, a parameter $\delta^{\rm L} \in [0, 1]$ is used to approximate the effect of blocking on the LoS probability by controlling the number of LoS paths, denoted as $N_{\rm L}$, in the considered area. As a result, the LoS probability in (37) is rewritten as

$$p_{kl}^{\rm L} = \begin{cases} 1, & \text{if } 0 < d_{kl} < 300(1 - \delta^{\rm L}) \\ 0, & \text{otherwise} \end{cases} \tag{38}$$

which is a binary variable and can be used for calculating the K-factor and the LSF coefficients.

Given the environment-related LoS probability $p_{kl}^{\rm L}$, PCM is capable of providing the large-scale CSI $\mathbf{h}_{kl}^{\rm L}$ and $\mathbf{R}_{kl}^{\rm N}$ which match the actual wireless channel better than that calculated based on the LoS probability in (38). The transmission performance can be improved by applying these environment-aware large-scale CSI to the signal processing and initial access schemes proposed in Section III and IV.

B. Small-Scale CSI-Aware Transmission Via FCM

The ultimate FCM $\mathcal{M}_{\rm FCM}$ is expected to provide the small-scale CSI $\mathbf{h}_{kl}^{\rm N}$ and $e^{\jmath\phi_{kl}}$ based on the current 3D location vectors $(\mathbf{c}_l^{\rm ap}, \mathbf{c}_k^{\rm ue})$ by the function $f_{\rm FCM}(\cdot|\mathcal{E})$ conditioned on the environment database $\mathcal{E}$. Together with the large-scale CSI obtained from the PCM, the complete channel $\mathbf{h}_{kl}$ and its angle domain representation $\mathbf{g}_{kl}$ can be obtained, i.e.,

$$\mathcal{M}_{\rm FCM}: \quad \{\mathbf{h}_{kl}, \mathbf{g}_{kl}\} = f_{\rm FCM}((\mathbf{c}_l^{\rm ap}, \mathbf{c}_u^{\rm ue})|\mathcal{E}). \tag{39}$$

It should be noted that the SE expression in (17) in Section III only provides an achievable lower bound of the SE when the channel hardening effect is prominent. With the help of the FCM $\mathcal{M}_{\rm FCM}$, an upper bound of the SE with perfect "FCM-aided" CSI $\{\mathbf{g}_{kl} : \forall k, l\}$ can be derived. To this end, we first rewrite the final estimate $\widehat{s}_k$ in (16) as

$$\widehat{s}_k = \underbrace{\mathbf{a}_k^{\rm H}\mathbf{b}_{kk}s_k}_{\text{Desired signal}} + \underbrace{\sum_{i=1, i\neq k}^{K} \mathbf{a}_k^{\rm H}\mathbf{b}_{ki}s_i}_{\text{Interference}} + \underbrace{n_k'}_{\text{Noise}} \tag{40}$$

where the first term is the desired signal obtained over a known channel. By combining interference and noise in one term, an upper bound of SE is obtained as follows.

Proposition 1: A SE upper bound of UE k with FCM-aided CSI is

$$\overline{\rm SE}_k^{\rm ul} = \mathbb{E}\left\{\log_2\left(1 + \overline{\rm SINR}_k^{\rm ul}\right)\right\} \quad \text{bit/s/Hz} \tag{41}$$

where the SINR is

$$\overline{\rm SINR}_k^{\rm ul} = \frac{p_k|\mathbf{a}_k^{\rm H}\overline{\mathbf{b}}_{kk}|^2}{\mathbf{a}_k^{\rm H}(\sum_{i=1, i\neq k}^{K} p_i\overline{\mathbf{b}}_{ki}\overline{\mathbf{b}}_{ki}^{\rm H} + \overline{\mathbf{F}}_k)\mathbf{a}_k} \tag{42}$$

with $\overline{\mathbf{b}}_{ki} = [\mathbf{v}_{k1}^{\rm H}\mathbf{D}_{k1}\mathbf{g}_{i1}, \ldots, \mathbf{v}_{kL}^{\rm H}\mathbf{D}_{kL}\mathbf{g}_{iL}]$ and $\overline{\mathbf{F}}_k = \frac{\sigma^2}{N}\text{diag}(\|\mathbf{D}_{k1}\mathbf{v}_{k1}\|^2, \ldots, \|\mathbf{D}_{kL}\mathbf{v}_{kL}\|^2)$.

Proof: The proof follows a similar approach as in [7, Coro. 5.10] but with angle domain receive-combined channels $\{\overline{\mathbf{b}}_{ki} : \forall k, i\}$ and combining vectors $\{\mathbf{v}_{kl} : \forall k, l\}$. ■

Similar to (20), the generalized Rayleigh quotient of $\overline{\mathsf{SINR}}_k^{\mathrm{ul}}$ in (42) allows computing the best LSFD vector $\overline{\mathbf{a}}_k^{\mathrm{opt}}$ that maximizes $\overline{\mathsf{SINR}}_k^{\mathrm{ul}}$, which is given as follows.

Corollary 1: The effective uplink SINR in (42) for UE k is maximized by

$$\overline{\mathbf{a}}_k^{\mathrm{opt}} = p_k \left(\sum_{i=1}^{K} p_i \overline{\mathbf{b}}_{ki} \overline{\mathbf{b}}_{ki}^{\mathrm{H}} + \overline{\mathbf{F}}_k \right)^{\dagger} \overline{\mathbf{b}}_{kk} \tag{43}$$

which leads to the maximum value $\overline{\mathsf{SINR}}_k^{\mathrm{ul}} = p_k \overline{\mathbf{b}}_{kk}^{\mathrm{H}} (\sum_{i=1}^{K} p_i \overline{\mathbf{b}}_{ki} \overline{\mathbf{b}}_{ki}^{\mathrm{H}} + \overline{\mathbf{F}}_k)^{\dagger} \overline{\mathbf{b}}_{kk}$.

Proof: The proof follows the results in [33, Lem. B.10] and [33, Lem. B.4]. ■

The SE upper bound in Proposition 1 is applicable to any receive combining vector $\mathbf{v}_{kl}$ and any channel model, including the one in (4) and the 6GPCM. One can choose the computationally efficient MR combing scheme with $\overline{\mathbf{v}}_{kl}^{\mathrm{mr}} = \mathbf{D}_{kl} \mathbf{g}_{kl}$ or the MMSE-type combining schemes with more sophisticated interference suppression capability, which are given as follows.

Lemma 3: At AP l with perfect angle domain CSI $\{\mathbf{g}_{il} : \forall i\}$, the local conditional data MSE $\mathbb{E}\{|s_k - \widehat{s}_{kl}|^2 | \{\mathbf{g}_{il} : \forall i\}\}$ for UE k is minimized by the following angle domain L-MMSE combining vector

$$\overline{\mathbf{v}}_{kl}^{\mathrm{l-mmse}} = p_k \left(\sum_{i=1}^{K} p_i \mathbf{g}_{il} \mathbf{g}_{il}^{\mathrm{H}} + \frac{\sigma^2}{N} \mathbf{I}_N \right)^{-1} \mathbf{D}_{kl} \mathbf{g}_{kl}. \tag{44}$$

Proof: The proof is similar as in Lemma 1 but with the local conditional data MSE $\mathbb{E}\{|s_k - \widehat{s}_{kl}|^2 | \{\mathbf{g}_{il} : \forall i\}\}$. ■

Analogously, we obtain the angle domain LP-MMSE combining scheme with perfect angle domain CSI as

$$\overline{\mathbf{v}}_{kl}^{\mathrm{lp-mmse}} = p_k \left(\sum_{i \in \mathcal{D}_l} p_i \mathbf{g}_{il} \mathbf{g}_{il}^{\mathrm{H}} + \frac{\sigma^2}{N} \mathbf{I}_N \right)^{-1} \mathbf{D}_{kl} \mathbf{g}_{kl}. \tag{45}$$

With the proposed upper-bound SE expression in Proposition 1 and the corresponding angle domain receive combining and LSFD schemes, we are able to evaluate the proposed channel map-based transmission design quantitatively, which is discussed in the next section.

VI. Results and Analysis

In this section, we will quantitatively evaluate our proposed angle domain signal processing and initial access schemes in Sections III–IV and the transmission design aided by the FCM and PCM in Section V, in terms of SE, EE, and NMSE. As illustrated in Fig. 3, we consider an urban microcell scenario where the buildings are taking the same exterior dimensions and layouts as that in the China Network Valley, Nanjing, China. There are L APs, each equipped with N antennas, mounted on the rooftops of the buildings offering an adequate network coverage, and K UEs distributed in the coverage area of $318 \times 330\,\mathrm{m}^2$ randomly following an independent and uniform distribution.

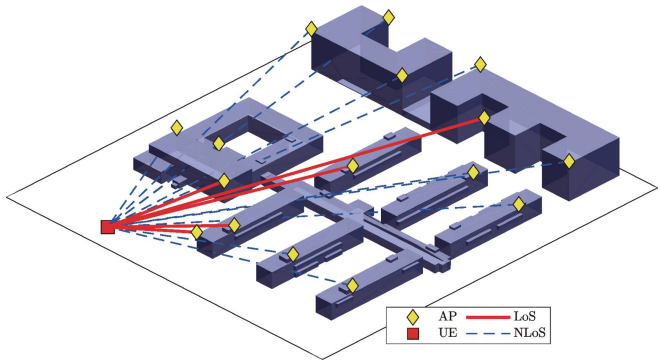

Fig. 3. Illustration of the considered communication scenario.

TABLE I
System Parameters

Parameters	Definitions	Values
L, K	Number of APs and UEs	16, 20
N	Number of antennas per AP	4
B	System bandwidth	20 MHz
τ_{c}, τ_{p}	Number of available channel uses and pilot sequences	200, 10
p_{p}, $p_{\max}$	Transmit power for pilots and maximal transmit power for data	0.1 W, 0.1 W
σ_φ, σ_θ	Standard deviation for AAOA and EAoA	10°, 10°

Unless otherwise specified, the adopted system parameters for simulation are given in Table I, the PCM is used to obtain the large-scale channel statistics, and the SE, EE, and NMSE are calculated with the channel model in (4) according to (17), (22), and (25), respectively.

A. Considered Schemes

To quantify the performance achieved by the proposed angle domain uplink receive combining, LSFD, pilot assignment, and AP selection design, we proposed several schemes, namely "O-Angle", "P-Angle", and "S-Angle". More precisely, O-Angle uses the L-MMSE combining in (14) and optimal LSFD in (20) where each AP serve all UEs, P-Angle uses the LP-MMSE combining in (15) and partial LSFD in (21) where each AP serve all UEs each AP serve τ_{p} UEs with the strongest channels, and S-Angle also uses the LP-MMSE combining in (15) while the LSFD vector and AP selection are obtained by solving the sparse optimization problem P_2 in (31). All the three aforementioned schemes employ the proposed similarity-based pilot assignment and operates in the angle domain. Analogically, we propose three space domain schemes corresponding to O-Angle and S-Angle, namely "O-Space" and "S-Space", respectively. Moreover, three space domain benchmark schemes are considered for comparison, namely "Scalable [10]", "Weighted [12]", and "Random", which are elaborated in Table II.

Additionally, we evaluate the transmission design aided by the FCM and PCM in Section V. In the case of utilizing the

TABLE II
THE CONSIDERED MULTIPLE ACCESS SCHEMES

Schemes	Domain	Combining	LSFD	Pilot Assignment	AP Selection
O-Angle	Angle	L-MMSE	Optimal LSFD	Obtained by solving P_1 in (28)	Each AP serves all UEs
O-Space	Space				
S-Angle	Angle	LP-MMSE	Obtained by solving P_2 in (31)		Obtained by solving P_2 in (31)
S-Space	Space				
P-Angle	Angle		Partial LSFD	–	Each AP serves τ_p UEs with the strongest channels
F-Angle					
Weighted [12]	Space			Heuristic scheme [12]	
Random				Random allocation	
Scalable [10]				Joint pilot assignment and AP selection scheme [10]	

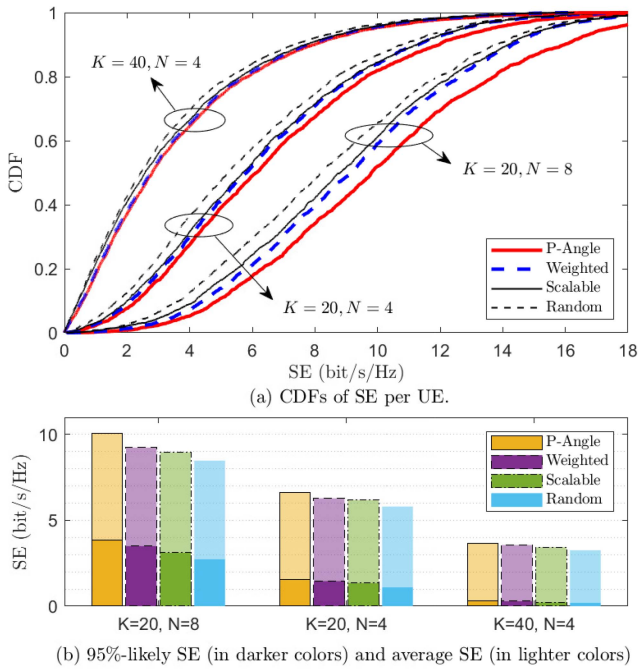

(a) CDFs of SE per UE.

(b) 95%-likely SE (in darker colors) and average SE (in lighter colors)

Fig. 4. (a) CDFs of SE per UE and (b) 95% -likely SE and average SE, considering different combinations of K and N.

FCM, we propose the scheme "F-Angle" where the pilot assignment is not needed due to the obviated channel estimation. As illustrated in Fig. 2, the FCM-aided CSI $\{\mathbf{g}_{kl} : \forall k, l\}$ is used for designing the angle domain transmission schemes where the SE is computed according to upper-bound expression in (41). In the case of utilizing the PCM, which is the default case where the channel estimation for the small-scale CSI is still needed and the used large-scale channel statistics are obtained with the LoS probability provided by the PCM. On the contrary, when neither the FCM nor PCM is used, the large-scale channel statistics used for channel estimation are obtained with the LoS probability computed according to (38).

B. Analysis for the Angle Domain Transmission

Fig. 4 demonstrates the SE performance considering different combination of the number of UEs K and the number of antennas per AP N, where the proposed scheme P-Angle is compared to the benchmark Graph, Scalable, and Random. More precisely, Fig. 4(a) depicts the cumulative distribution functions (CDFs) of the uplink SE per UE and Fig. 4(b) quantifies the corresponding 95% -likely SE and average SE, where the average SE values are larger than the 95% -likely SE values and drawn in lighter colors in the histogram. The first observation is that P-Angle outperforms the benchmark on both 95% -likely SE and average SE in every considered case with respect to K and N. This is expected since the interference caused by pilot reuse is effectively suppressed by P-Angle where the similarities between UEs are revealed more prominently in the angle domain to be exploited to find the best pilot assignment with the minimum overall interference in (28). By comparing the case with $K = 20, N = 4$ and that with $K = 40, N = 4$, it can be seen that the former outperforms the latter by around $1.8\times$ on average SE and around $5.6\times$ on 95% -likely SE thanks to the reduced inter-UE interference by having fewer serving UEs. Taking the case with $K = 20, N = 4$ as a baseline, the average SE is further improved to around $1.5\times$ and the 95% -likely SE is further improved to around $2.4\times$ in the case with $K = 20, N = 8$. This comes from the enhanced interference suppression gain of the LP-MMSE combiner by having more antennas per AP. Additionally, we notice that the performance gaps between P-Angle and the most competitive benchmark Weighted are widened in the "preferable" cases. For instance, compared to Weighted, P-Angle achieves a 9.1% improvement in average SE when $K = 20, N = 8$, and this improvement shrinks to 2.3% when $K = 40, N = 4$ since the performances of both schemes are limited in an inferior case.

Considering the same schemes and benchmark as Fig. 4 with $K = 20, N = 4$, Fig. 5(a) and (b) further discuss the impact of the number of pilots τ_{p} on the average NMSE and average SE, respectively. Similar to Fig. 4, P-Angle demonstrates its advantages over the benchmark on both average NMSE and average SE for the same reason as explained in Fig. 4. Then, we notice that the average NMSE decreases monotonically as τ_{p} increases, which is consistent with (25) since the matrix $\mathbf{\Psi}_{\iota_k l}$ is likely to include fewer undesired UEs' statistical CSI during the channel estimation when there are more available pilot sequences. Moreover, we observe that the average SE is a concave function with respect to τ_{p}. The reason is that increasing

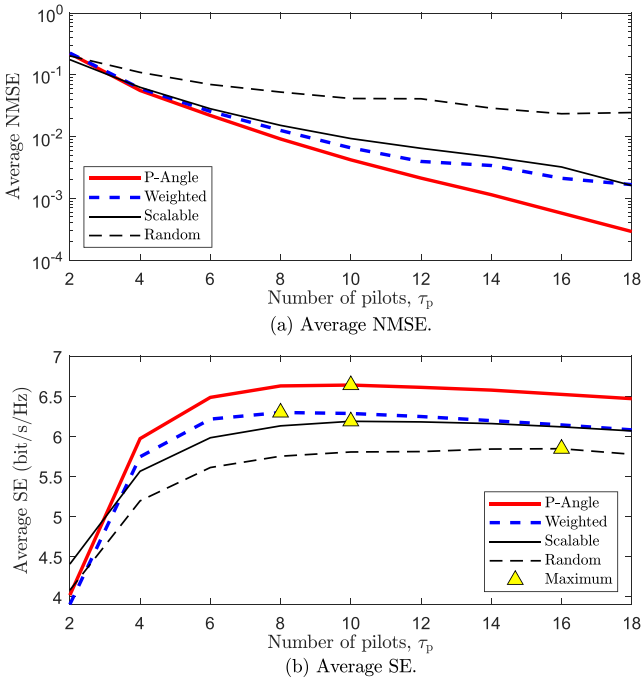

(a) Average NMSE.

(b) Average SE.

Fig. 5. (a) Average NMSE and (b) average SE versus τ_p.

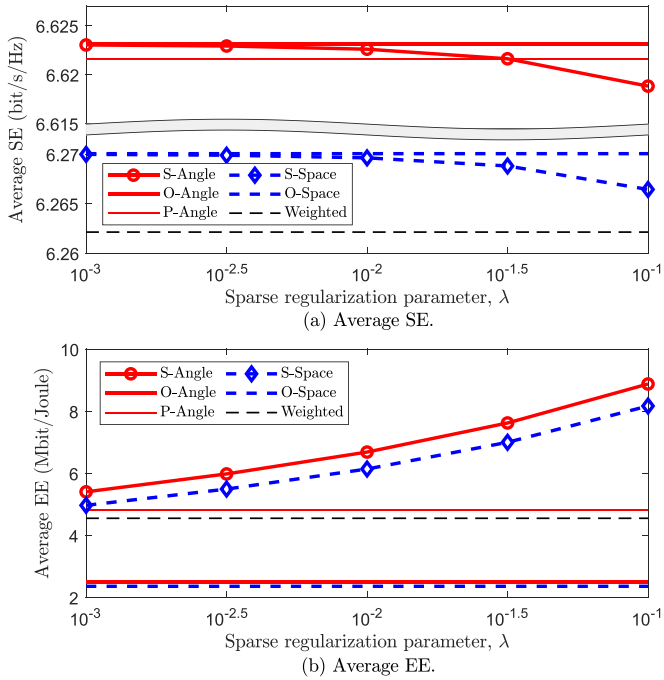

(a) Average SE.

(b) Average EE.

Fig. 6. (a) Average SE and (b) average EE versus λ, considering different operation domains.

τ_p not only promotes the SINR SINR_k but also reduces the prelog factor $\frac{\tau_u}{\tau_c} = 1 - \frac{\tau_p}{\tau_c}$ in (17). The former effect dominates in the region of insufficient available pilots and causes the escalation of average SE with the increased τ_p until the saturation point (i.e., the Maximum) is reached. Henceforth, the latter effect starts to dominate and increasing τ_p will do more harm than good on average SE. The benefits obtained by the proposed angle domain similarity-based pilot assignment has been exhibited in Figs. 4 and 5. In Fig. 6, we evaluate the proposed sparsity-induced AP selection in terms of average SE and average EE considering the angle domain schemes (i.e., O-Angle, P-Angle, and S-Angle) and the space domain schemes (i.e., O-Space and S-Space) for various values of the regularization parameter λ. Since Weighted behaves as the most competitive benchmark in Figs. 4 and 5, we only include Weighted into the comparisons in Fig. 6 for concise presentation. Note that Weighted operates in the space domain as well. Fig. 6(a) is dedicated to average SE where the vertical axis is broke and the unnecessary blank space is removed for clear presentation due to the large SE gaps between the angle domain schemes and space domain schemes. We first observe that the average SE decreases as λ increases. The average SE loss is marginal since each UE is served by a subset of APs that contribute the most during the LSFD. Consequently, a significant average EE improvement is achieved due to the reduced power consumption. For instance, compared to O-Angle where each AP served all UEs, S-Angle achieves a $3.6\times$ average EE with an average SE loss of less than 1% when $\lambda = 10^{-1}$. Compared to P-Angle, S-Angle achieves a $1.6\times$ average EE and almost identical average SE when $\lambda = 10^{-1.5}$, and this average EE improvement increases to $1.8\times$ with an average SE loss of less than 1% when $\lambda = 10^{-1}$. This comes from the joint optimization of the LSFD and AP selection design utilized in S-Angle, which outperforms the separate LSFD and AP selection design utilized in P-Angle. Similar trends in average SE and average EE concerning λ observed in the angle domain schemes can be observed in the space domain as well. When comparing the schemes operated in different domains, the average EE of the angle domain schemes is around 8.0% higher than that of their space domain alternatives due to the higher achieved average SE.

C. Analysis for the Channel Map-Aided Transmission

Fig. 7 demonstrates the SE performance by comparing the proposed scheme P-Angle with the most competitive benchmark Weighted considering two cases: 1) case "w/ PCM" that exploits the channel statistics provided by the PCM for designing transmission schemes and 2) case "w/o PCM" that exploits the channel statistics obtained with the help of the LoS probability computed according to (38). The LoS probability in case w/o PCM takes the same value as that of the average LoS probability in case w/ PCM for a fair comparison. Moreover, the impact of channel model on the SE performance is also demonstrated by considering scheme "F-Angle (6GPCM)" where the 6GPCM is adopted. Similar to Fig. 4, the CDFs of SE per UE, 95% -likely SE, and average SE are regarded as performance metrics. We first observe that P-Angle outperforms Weighted in both cases w/ PCM and w/o PCM. Then, better SE performance is observed when utilizing the PCM, which assists the transmission by providing the a priori environment-related large-scale channel statistics. More precisely, the average SE and 95% -likely SE of the schemes in case w/ PCM are around 9.8% and 36.0%

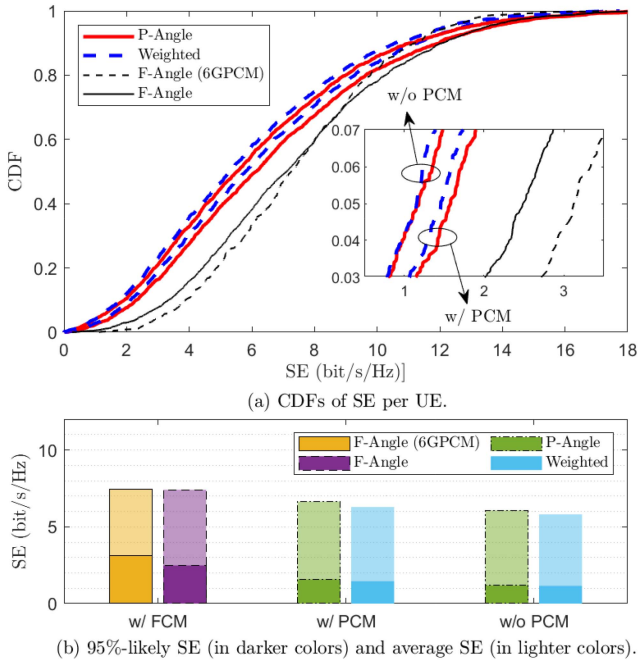

(a) CDFs of SE per UE.

(b) 95%-likely SE (in darker colors) and average SE (in lighter colors).

Fig. 7. (a) CDFs of SE per UE and (b) 95% -likely SE and average SE, considering different channel maps.

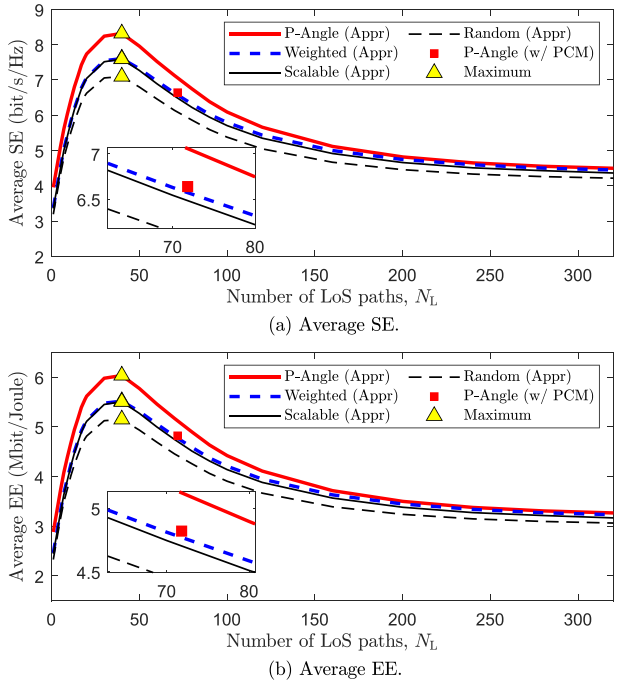

(a) Average SE.

(b) Average EE.

Fig. 8. (a) Average SE and (b) average EE versus N_{L}, considering different channel maps.

higher than that of the schemes in case w/o PCM, respectively. Note that these performance improvements will decay as the localization error increases due to the inaccurate LoS probabilities in practice. Then, the SE performance is further improved by employing the FCM which provides the complete CSI on the basis of the PCM. Taking P-Angle in case w/o PCM as a baseline, F-Angle further increases the average SE and 95% -likely SE improvements to 22.0% and 110.2% , respectively. Compared to scheme F-Angle, F-Angle (6GPCM) achieves the similar average SE but 25.0% higher 95% -likely SE, implying that the channel realizations modeled by 6GPCM is more uniform than that modeled by (4).

In Fig. 8, we investigate the impact of number of LoS paths, i.e., N_{L}, on the average SE and average EE in Fig. 8(a) and (b), respectively. The value of N_{L} could range from 0 to 320 with $L = 16$ APs and $K = 20$ UEs. For the considered scenario illustrated in Fig. 3 where the layouts of APs and buildings are fixed, N_{L} is hardly possible to go through the aforemention range when the UEs are independently and uniformly distributed in the coverage area. Therefore, we consider a case marked as "Appr", where the large-scale channel statistics used for generate the *approximate* "ground-truth" CSI are obtained with the LoS probability in (38) as well. Therefore, the case Appr can be regarded as a PCM-aided case based on the approximate "ground-truth" CSI. The parameter δ^{L} is used to keep N_{L} between 0 and 320. It can be seen in Fig. 7(a) that the average SE is a concave function with respect to N_{L}, where the deteriorations in average SE appear when N_{L} approaches either 0 or 320. The reason is that the received signal strength is week when the LoS paths are missing, that reduces the average SE; on the opposite, too many LoS paths will cause undesirable interference between the UEs, which also causes an average SE reduction. In Fig. 7(b), we notice that the average EE is also a concave function concerning N_{L} for the similar reason as that in Fig. 7(a). By comparing P-Angle (w/ PCM) with P-Angle (Appr) when N_{L} is 71.8, which is the average N_{L} of the considered scenario in Fig. 3, the interesting observation is that P-Angle (Appr) achieves a higher average SE than P-Angle (w/ PCM). This comes from the fact that the overall received signal strength in case w/ PCM is weaker than that in case Appr due to actual building blocking, which lengthens the average distances of the LoS paths when the both cases have the same N_{L}. That is to say, the actual propagation environment needs to be considered during the transmission scheme design to avoid overestimating the achievable SE and EE performance.

In Fig. 9, the average SE and EE of the angle domain schemes (i.e., O-Angle and S-Angle) and the benchmark Weighted are demonstrated to highlight the achieved good SE-EE trade-offs with various values of λ in case w/o PCM. Additionally, F-Angle (6GPCM) and F-Angle are included in comparison as well. Together with Fig. 6 which presents the average SE and EE in case w/ PCM, the impact of the a priori CSI provided by different channel maps is discussed. Comparing with Fig. 6(a), we first observe that the average SE of S-Angle (w/o PCM) decreases as λ increases and the average SE loss compared to O-Angle (w/o PCM) is less than 1% , which are consistent with that in case w/ PCM for the similar reason. Moreover, the average SE of O-Angle (w/o PCM) is 5.6% higher than that of Weighted (w/o PCM). This average SE improvement is further increased to around 31.6% by F-Angle (6GPCM) and F-Angle thanks to the provided the complete CSI, where the average SE of F-Angle (6GPCM) is *slightly* higher than that

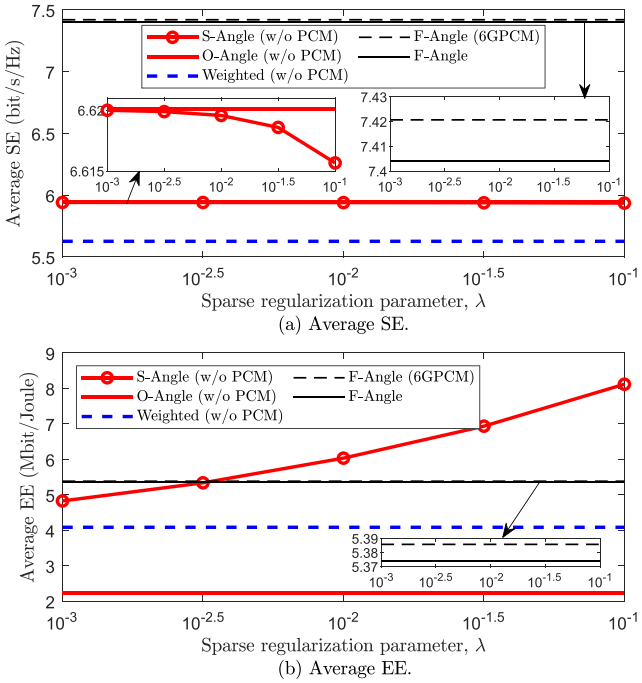

Fig. 9. (a) Average SE and (b) average EE versus λ, considering different channel maps.

of F-Angle. Similar to that in case w/ PCM, the average EE of S-Angle (w/o PCM) increases as λ increases due to the reduced power consumption. Taking $\lambda = 10^{-1}$ as an example, compared to F-Angle (6GPCM), Weighted (w/o PCM), and O-Angle (w/o PCM), S-Angle (w/o PCM) improves the average EE to $1.5\times$, $2.0\times$, and $3.6\times$, respectively. Furthermore, it can be seen that the average EE of F-Angle (6GPCM) is *slightly* higher than that of F-Angle, and is $1.3\times$ and $2.4\times$ that of Weighted (w/o PCM) and O-Angle (w/o PCM), respectively.

VII. Conclusion

This paper has proposed a channel map-based angle domain multiple access scheme for uplink CF M-MIMO communications. A two-stage data reception scheme dedicated to angle domain CF M-MIMO has been proposed where the angle domain MMSE-type receive combing and LSFD vectors are derived. Based on this, an angle domain initial access strategy, including pilot assignment and AP selection, has been developed to suppress the overall interference and reduce unnecessary power consumption under the guidance of the derived access criterion. Simulation results have demonstrated that the proposed angle domain schemes effectively improve the SE performance and offer a better SE-EE trade-off compared to their space domain alternatives. Moreover, two channel map-based transmission mechanisms aided by PCM and the ultimate FCM have been constructed with a tailored data reception scheme consisting of the newly derived upper-bound SE expression with MMSE-type combining and LSFD vectors. Results have shown that the channel map-based schemes can further boost transmission performance compared to the schemes without using channel maps, verifying the positive effects by being aware of the channel and exploiting the appropriate CSI.

Appendix A
Proof of Lemma 2

According to the definition of NMSE_k in (25), the definition of $\widetilde{\boldsymbol{\Psi}}_{\iota_k l}$ in (26), we have

$$\operatorname{tr}\left(\mathbf{D}_{kl}\boldsymbol{\Omega}_{kl}\mathbf{U}^{\mathrm{H}}\boldsymbol{\Psi}_{\iota_k l}^{-1}\mathbf{U}\boldsymbol{\Omega}_{kl}\right) \tag{46}$$

$$= \operatorname{tr}\left(\mathbf{D}_{kl}\boldsymbol{\Omega}_{kl}\mathbf{U}^{\mathrm{H}}\left(\widetilde{\boldsymbol{\Psi}}_{\iota_k l}+\widetilde{\boldsymbol{\Omega}}_{kl}^{\mathrm{res}}\right)^{-1}\mathbf{U}\boldsymbol{\Omega}_{kl}\right) \tag{47}$$

$$\leq \operatorname{tr}\left(\mathbf{U}\boldsymbol{\Omega}_{kl}\mathbf{D}_{kl}\boldsymbol{\Omega}_{kl}\mathbf{U}^{\mathrm{H}}\widetilde{\boldsymbol{\Psi}}_{\iota_k l}^{-1}\right) \tag{48}$$

where $\widetilde{\boldsymbol{\Omega}}_{kl}^{\mathrm{res}} = \tau_{\mathrm{p}}p_{\mathrm{p}}\sum_{i\in\mathcal{S}_{\iota_k}\setminus\{k\}}\mathbf{U}\boldsymbol{\Omega}_{il}\mathbf{U}^{\mathrm{H}}$, the inequality in (48) comes from the results in [7, Lem. B.4], and the equality occurs when

$$\widetilde{\boldsymbol{\Omega}}_{kl}^{\mathrm{res}}\widetilde{\boldsymbol{\Psi}}_{\iota_k l}^{-1}\mathbf{U}\boldsymbol{\Omega}_{kl}\mathbf{D}_{kl}\boldsymbol{\Omega}_{kl}\mathbf{U}^{\mathrm{H}} = \mathbf{0}. \tag{49}$$

With the help of the results in [33, Lem. B.5] and the definition of steering matrix $\mathbf{U}$, we rewrite the condition in (49) as

$$\tau_{\mathrm{p}}p_{\mathrm{p}}\sum_{i\in\mathcal{S}_{\iota_k}\setminus\{k\}}\mathbf{U}\mathbf{D}_{kl}\boldsymbol{\Omega}_{il}\boldsymbol{\Omega}_{kl}\left(\tau_{\mathrm{p}}p_{\mathrm{p}}\boldsymbol{\Omega}_{kl}+\frac{\sigma^2}{N}\mathbf{I}_N\right)^{-1}\boldsymbol{\Omega}_{kl}\mathbf{U}^{\mathrm{H}}=\mathbf{0} \tag{50}$$

which holds when one of the conditions in Lemma 2 is satisfied, and the lower bound in (26) is therefore achieved. This completes the proof.

References

[1] S. Chen, C.-X. Wang, J. Li, C. Huang, H. Chang, and Y. Chen, "Improving cell-free massive MIMO through channel map-based angle domain multiple access," in *Proc. IEEE Int. Conf. Commun.*, Canada, accepted for publication, 2025.
[2] C.-X. Wang et al., "On the road to 6G: Visions, requirements, key technologies, and testbeds," *IEEE Commun. Surveys Tuts.*, vol. 25, no. 2, pp. 905–974, Secondquarter 2023.
[3] W. Saad, M. Bennis, and M. Chen, "A vision of 6G wireless systems: Applications, trends, technologies, and open research problems," *IEEE Netw.*, vol. 34, no. 3, pp. 134–142, May/Jun. 2020.
[4] S. Chen, J. Zhang, J. Zhang, E. Björnson, and B. Ai, "A survey on user-centric cell-free massive MIMO systems," *Digit. Commun. Netw.*, vol. 8, no. 5, pp. 695–719, Oct. 2022.
[5] Z. Wang et al., "A tutorial on extremely large-scale MIMO for 6G: Fundamentals, signal processing, and applications," *IEEE Commun. Surveys Tuts.*, vol. 26, no. 3, pp. 1560–1605, thirdquarter 2024.
[6] C.-X. Wang, Y. Yang, J. Huang, X. Gao, T. J. Cui, and L. Hanzo, "Electromagnetic information theory: Fundamentals and applications for 6G wireless communication systems," *IEEE Wireless Commun.*, vol. 31, no. 5, pp. 279–286, Oct. 2024.
[7] Ö. T. Demir, E. Björnson, and L. Sanguinetti, "Foundations of user-centric cell-free massive MIMO," *Found. Trends Signal Process.*, vol. 14, no. 3-4, pp. 162–472, 2021.
[8] S. Chen, J. Zhang, E. Björnson, J. Zhang, and B. Ai, "Structured massive access for scalable cell-free massive MIMO systems," *IEEE J. Sel. Areas Commun.*, vol. 39, no. 4, pp. 1086–1100, Apr. 2021.
[9] S. Chen, J. Zhang, E. Björnson, Ö. T. Demir, and B. Ai, "Energy-efficient cell-free massive MIMO through sparse large-scale fading processing," *IEEE Trans. Wireless Commun.*, vol. 22, no. 12, pp. 9374–9389, Dec. 2023.
[10] E. Björnson and L. Sanguinetti, "Scalable cell-free massive MIMO systems," *IEEE Trans. Commun.*, vol. 68, no. 7, pp. 4247–4261, Jul. 2020.
[11] S. Chen, J. Zhang, E. Björnson, and B. Ai, "Improving fairness for cell-free massive MIMO through interference-aware massive access," *IEEE Trans. Veh. Technol.*, vol. 72, no. 4, pp. 5468–5472, Apr. 2023.

[12] W. Zeng, Y. He, B. Li, and S. Wang, "Pilot assignment for cell-free massive MIMO systems using a weighted graphic framework," *IEEE Trans. Veh. Technol.*, vol. 70, no. 6, pp. 6190–6194, Jun. 2021.
[13] A. Al Ayidh, Y. Sambo, and M. A. Imran, "Mitigation pilot contamination based on matching technique for uplink cell-free massive MIMO systems," *Sci. Rep.*, vol. 12, no. 1, 2022, Art. no. 16893.
[14] Y. Gao, H. Hu, J. Chen, X. Wang, X. Chu, and J. Zhang, "A matching-based pilot assignment algorithm for cell-free massive MIMO networks," *IEEE Trans. Veh. Technol.*, vol. 73, no. 1, pp. 1453–1457, Jan. 2024.
[15] R. Feng, C.-X. Wang, J. Huang, X. Gao, S. Salous, and H. Haas, "Classification and comparison of massive MIMO propagation channel models," *IEEE Internet J.*, vol. 9, no. 23, pp. 23452–23471, Dec. 2022.
[16] H. Xie, F. Gao, S. Zhang, and S. Jin, "A unified transmission strategy for TDD/FDD massive MIMO systems with spatial basis expansion model," *IEEE Trans. Veh. Technol.*, vol. 66, no. 4, pp. 3170–3184, Apr. 2017.
[17] M. Li, S. Zhang, F. Gao, P. Fan, and O. A. Dobre, "A new path division multiple access for the massive MIMO-OTFS networks," *IEEE J. Sel. Areas Commun.*, vol. 39, no. 4, pp. 903–918, Apr. 2021.
[18] J. Yang, A.-A. Lu, Y. Chen, X. Gao, X.-G. Xia, and D. T. M. Slock, "Channel estimation for massive MIMO: An information geometry approach," *IEEE Trans. Signal Process.*, vol. 70, pp. 4820–4834, 2022.
[19] Z. Wang, C. Qian, L. Dai, J. Chen, C. Sun, and S. Chen, "Location-based channel estimation and pilot assignment for massive mimo systems," in *Proc. IEEE Int. Conf. Commun. Workshop*, 2015, pp. 1264–1268.
[20] L. S. Muppirisetty, T. Charalambous, J. Karout, G. Fodor, and H. Wymeersch, "Location-aided pilot contamination avoidance for massive MIMO systems," *IEEE Trans. Wireless Commun.*, vol. 17, no. 4, pp. 2662–2674, Apr. 2018.
[21] C. Sun, X. Gao, S. Jin, M. Matthaiou, Z. Ding, and C. Xiao, "Beam division multiple access transmission for massive MIMO communications," *IEEE Trans. Commun.*, vol. 63, no. 6, pp. 2170–2184, Jun. 2015.
[22] H. Chang et al., "A novel 3D beam domain channel model for UAV massive MIMO communications," *IEEE Trans. Wireless Commun.*, vol. 22, no. 8, pp. 5431–5445, Aug. 2023.
[23] H. Chang, C.-X. Wang, R. Feng, C. Huang, L. Hou, and E.-H. M. Aggoune, "Beam domain channel modeling and prediction for UAV communications," *IEEE Trans. Wireless Commun.*, vol. 24, no. 2, pp. 969–983, Feb. 2025.
[24] C.-X. Wang, Z. Lv, X. Gao, X. You, Y. Hao, and H. Haas, "Pervasive wireless channel modeling theory and applications to 6G GBSMs for all frequency bands and all scenarios," *IEEE Trans. Veh. Technol.*, vol. 71, no. 9, pp. 9159–9173, Sep. 2022.
[25] C.-X. Wang, Z. Lv, Y. Chen, and H. Haas, "A complete study of space-time-frequency statistical properties of the 6G pervasive channel model," *IEEE Trans. Commun.*, vol. 71, no. 12, pp. 7273–7287, Dec. 2023.
[26] Y. Zeng and X. Xu, "Toward environment-aware 6G communications via channel knowledge map," *IEEE Wireless Commun.*, vol. 28, no. 3, pp. 84–91, Jun. 2021.
[27] Y. Zeng et al., "A tutorial on environment-aware communications via channel knowledge map for 6G," *IEEE Commun. Surveys Tut.*, vol. 26, no. 3, pp. 1478–1519, thirdquarter 2024.
[28] D. Wu, Y. Zeng, S. Jin, and R. Zhang, "Environment-aware hybrid beamforming by leveraging channel knowledge map," *IEEE Trans. Wireless Commun.*, vol. 23, no. 5, pp. 4990–5005, May 2024.
[29] H. Li, P. Li, J. Xu, J. Chen, and Y. Zeng, "Derivative-free placement optimization for multi-UAV wireless networks with channel knowledge map," in *Proc. IEEE Int. Conf. Commun. Workshops*, Seoul, Korea, Republic of, Jun. 2022, pp. 1029–1034.
[30] Y. Long, Y. Zeng, X. Xu, and Y. Huang, "Environment-aware wireless localization enabled by channel knowledge map," in *Proc. 2022 IEEE Glob. Commun. Conf.*, Rio de Janeiro, Brazil, Dec. 2022, pp. 5354–5359.
[31] T. Qi, C. Huang, J. Shi, J. Li, S. Chen, and C.-X. Wang, "A novel dynamic channel map for 6G MIMO communications," in *Proc. IEEE/CIC Int. Conf. Commun. China*, Hangzhou, China, Aug. 2024, pp. 809–814.
[32] 3GPP, "Spatial channel model for multiple input multiple output (MIMO) simulations (Release 18)," 3GPP, Tech. Rep. TR 25.996, V18.0.0, Mar. 2024.
[33] E. Björnson, J. Hoydis, and L. Sanguinetti, "Massive MIMO networks: Spectral, energy, and hardware efficiency," *Found. Trends Signal Process.*, vol. 11, no. 3–4, pp. 154–655, 2017.
[34] S. Sahni and T. Gonzalez, "P-complete approximation problems," *J. ACM*, vol. 23, no. 3, pp. 555–565, Jul. 1976.
[35] I. Rish and G. Grabarnik, *Sparse Modeling: Theory, Algorithms, and Applications*. Boca Raton, FL, USA: CRC Press, 2014.
[36] CVX Research Inc., "CVX: Matlab software for disciplined convex programming, academic users," 2015. [Online]. Available: http://cvxr.com/cvx/

Shuaifei Chen (Member, IEEE) received the B.S. degree in communication engineering and the Ph.D. degree in information and communication engineering from Beijing Jiaotong University, Beijing, China, in 2018 and 2023, respectively. From 2019 to 2020, he visited the Department of Communication Systems, Linköping University, Linköping, Sweden. From 2021 to 2022, he visited the Division of Communication Systems, KTH Royal Institute of Technology, Stockholm, Sweden. He is currently a Research Fellow with the Pervasive Communication Research Center, Purple Mountain Laboratories, Nanjing, China, and also a Postdoctoral Researcher with the National Mobile Communications Research Laboratory, School of Information Science and Engineering, Southeast University, Nanjing. His research interests include signal processing and resource allocation for wireless communications, cell-free massive MIMO, and channel map-aided 6G multiple antenna technologies. He was recognized as an Exemplary Reviewer of IEEE TRANSACTIONS ON COMMUNICATIONS in 2021 and IEEE COMMUNICATIONS LETTERS in 2023.

Cheng-Xiang Wang (Fellow, IEEE) received the B.Sc. and M.Eng. degrees in communication and information systems from Shandong University, Jinan, China, in 1997 and 2000, respectively, and the Ph.D. degree in wireless communications from Aalborg University, Aalborg, Denmark, in 2004. From 2000 to 2001, he was a Research Assistant with the Hamburg University of Technology, Hamburg, Germany, Visiting Researcher with Siemens AG Mobile Phones, Munich, Germany, in 2004, and Research Fellow with the University of Agder, Grimstad, Norway, from 2001 to 2005. From 2005 to 2018, he was with Heriot-Watt University, Edinburgh, U.K., where he was promoted to a Professor in 2011. Since 2018, he has been with Southeast University, Nanjing, China, as a Professor, and he is currently the Executive Dean with the School of Information Science and Engineering. He is also a Professor with Pervasive Communication Research Center, Purple Mountain Laboratories, Nanjing, China. He has authored four books, three book chapters, and more than 620 papers in refereed journals and conference proceedings, including 28 highly cited papers. He has also delivered 32 invited keynote speeches/talks and 21 tutorials in international conferences. He is also a Highly-Cited Researcher recognized by Clarivate Analytics during 2017–2020. His research interests include wireless channel measurements and modeling, 6G wireless communication networks, and electromagnetic information theory. He is also an Executive Editorial Committee Member with the IEEE TRANSACTIONS ON WIRELESS COMMUNICATIONS. from 2007 to 2009, he was the Editor for more than sixteen international journals, including the IEEE TRANSACTIONS ON WIRELESS COMMUNICATIONS, IEEE TRANSACTIONS ON VEHICULAR TECHNOLOGY, from 2011 to 2017, and IEEE TRANSACTIONS ON COMMUNICATIONS, from 2015 to 2017. He was a Guest Editor of the IEEE JOURNAL ON SELECTED AREAS IN COMMUNICATIONS, IEEE TRANSACTIONS ON BIG DATA, and IEEE TRANSACTIONS ON COGNITIVE COMMUNICATIONS AND NETWORKING. He was a TPC Chair and General Chair for more than 30 international conferences. Dr. Wang was the recipient of the IEEE Neal Shepherd Memorial Best Propagation Paper Award in 2024 and 19 Best Paper awards from international conferences. He is a Member of the Academia Europaea (The Academy of Europe) and European Academy of Sciences and Arts (EASA), a Fellow of the Royal Society of Edinburgh (FRSE), IET, and IEEE Communications Society Distinguished Lecturer in 2019 and 2020.

Junling Li (Member, IEEE) received the B.S. degree from Tianjin University, Tianjin, China, and the M.S. degree from the Beijing University of Posts and Telecommunications, Beijing, China, in 2013 and 2016, respectively, the Ph.D. degree from the Department of Electrical and Computer Engineering, University of Waterloo, Waterloo, ON, Canada, in 2020. She was a Joint Postdoctoral Research Fellow with the Shenzhen Institute of Artificial Intelligence and Robotics for Society (AIRS), University of Waterloo, and was also with the Chinese University of Hong Kong, Shenzhen, China, from 2020 to 2022. She is currently an Associate Professor with the National Mobile Communications Research Laboratory, Southeast University, Nanjing, China. Her research interests include digital twin, channel modeling, game theory, and machine learning-based channel prediction. Dr. Li was the recipient of the Best Paper Award at the IEEE ICCC 2019 and ICCT 2023.

Chen Huang (Member, IEEE) received the Ph.D. degree from Beijing Jiaotong University, Beijing, China, in 2021. From 2018 to 2020, he was a Visiting Scholar with the University of Southern California (USC), Los Angeles, CA, USA and was also with the Universite Catholique de Louvain (UCL), Louvain-la-Neuve, Belgium. From April 2021 to April 2023, he was a Postdoctoral Research Associate with Pervasive Communication Research Center, Purple Mountain Laboratories (PML), Nanjing, China, and was also with the National Mobile Communications Research Laboratory, School of Information Science and Engineering, Southeast University (SEU), Nanjing, China. Since April 2023, he has been an Research Associate Professor with Pervasive Communication Research Center, PML, and an Extramural Supervisor with the National Mobile Communications Research Laboratory, School of Information Science and Engineering, SEU, China. He has authored/co-authored one book chapters, more than 60 journal and conference papers, as well as 17 patents. His research interests include 6G channel measurements, characterization, and modeling, machine learning-based channel prediction, and localization. Dr. Huang was selected in Young Elite Scientists Sponsorship Program by China Association for Science and Technology and Outstanding Postdoctoral Fellow Program in Jiangsu, was the recipient of the four times the Best Paper Award from IEEE/CIC ICCC 2024, IEEE ICCT2023, WCSP 2018, and IEEE/CIC ICCC 2018. He is also the Associate Editor for IEEE TRANSACTIONS ON VEHICULAR TECHNOLOGY. He is the Technical Program Committee (TPC) Member for several conferences, including GlobeCom, ICC, VTC-fall, and VTC-spring.

Hengtai Chang (Member, IEEE) received the B.Sc. and Ph.D. degrees from the School of Information Science and Engineering, Shandong University, Jinan, China, in 2016 and 2021, respectively. He was a Postdoctoral Research Associate with Purple Mountain Laboratories, China, and was also with China National Mobile Communications Research Laboratory, Southeast University, Nanjing, China, from 2021 to 2024. Since 2024, he has been an Associate Professor with the School of Information Science and Engineering, Shandong University. His research interests include UAV communications, wireless propagation channel measurements and channel modeling, and B5G/6G wireless communications.

Yusong Huang received the B.E. degree in information engineering in 2023 from Southeast University, Nanjing, China,, where he is currently working toward the M.Sc. degree with the National Mobile Communications Research Laboratory. His research interests include channel characteristics and communication system performance analysis.

Jie Huang (Member, IEEE) received the B.E. degree in information engineering from Xidian University, Xi'an, China, in 2013, and the Ph.D. degree in information and communication engineering from Shandong University, Jinan, China, in 2018. From 2018 to 2020, he was a Postdoctoral Research Associate with the National Mobile Communications Research Laboratory, Southeast University, Nanjing, China, supported by the National Postdoctoral Program for Innovative Talents. From January 2019 to February 2020, he was a Postdoctoral Research Associate with Durham University, Durham, U.K. Since March 2019, he has been a Part-Time Researcher with Purple Mountain Laboratories, Nanjing, China. Since November 2020, he has been an Associate Professor with the National Mobile Communications Research Laboratory, Southeast University. He has authored and co-authored more than 120 papers in refereed journals and conference proceedings. He has delivered more than ten tutorials in international conferences, including IEEE Globecom and IEEE ICC. His research interests include millimeter wave, massive MIMO, reconfigurable intelligent surface channel measurements and modeling, electromagnetic information theory, and 6G wireless communications. He was the recipient of the IEEE Neal Shepherd Memorial Best Propagation Paper Award in 2024 and Best Paper awards from WPMC 2016, WCSP 2020, WCSP 2021, and WCSP 2024.

Yunfei Chen (Senior Member, IEEE) received the B.E. and M.E. degrees in electronics engineering from Shanghai Jiaotong University, Shanghai, China, in 1998 and 2001, respectively, and the Ph.D. degree from the University of Alberta, Edmonton, AB, Canada, in 2006. He is currently a Professor with the Department of Engineering, Durham University, Durham, U.K. His research interests include wireless communications, performance analysis, joint radar communications designs, cognitive radios, wireless relaying, and energy harvesting.